EFFECT OF THERMOMECHANICAL TREATMENTS

ON THE TRANSFORMATION BEHAVIOR OF A TiNi ALLOY

BY

Kuang-Hua Hou

A THESIS

Submitted to
Michigan State University
in partial fulfillment of the requirements
for the degree of

MASTER OF SCIENCE

Department of Metallurgy, Mechanics and Materials Science

1986

ABSTRACT

EFFECT OF THERMOMECHANICAL TREATMENT ON TRANSFORMATION BEHAVIOR OF A TiNi ALLOY

BY

Kuang-Hua Hou

The transformation behavior of a TiNi alloy has been studied by using electrical resistance vs. temperature curves obtained from different thermomechanically treated specimens. Transmission electron microscopy and electron diffraction were also employed to observed the microstructures of specimens. Effects of aging time, aging temperature, cooling rate, thermal cycling, cold rolling and annealing after cold rolling were investigated. By combining the effects of different variables, the controlling factors of transformation behavior of this alloy have been determined to be the formation of precipitates and the introduction of dislocations. The former affects the composition of the matrix and the latter affects the formation of martensite plates. Premartensitic transformation has been investigated by TEM. Charge density wave influences the structure of parent B2 phase by changing it to incommensurate or commensurate phases. Premartensitic transformation can be enhanced by aging treatments.

TABLE OF CONTENTS

ACKNOWLEDGEMENTS

The author wishes to express sincere appreciation to Dr. C. M. Hwang for his patient guidance and encouraging advices during this research.

The help from my friend Pei-San Yu is very much appreciated.

This thesis is to my dearest parents.

LIST OF TABLES

LIST OF FIGURES

Figure page

Figure page

Figure page

Figure | page

I. INTRODUCTION

The binary TiNi alloys have been known as shape memory alloys since their unusual shape memory effect (SME) was reported in 1962 by William J. Buehler of the U.S. Naval Ordance Laboratory. Extensive studies of TiNi alloys have been done in order to understand the mechanisms of SME and its related transformations. Besides SME, pseudoelasticity and "two way" shape memory effect are also studied as important characteristics which make TiNi alloys as the most promising alloys in industrial as well as medical applications (1-5).

The high temperature parent phase of TiNi has already been determined as having CsCl (B2) structure (6-15). As TiNi is cooled from parent phase to just above Martensite start temperature (Ms), it will exhibit some anomalies in physical properties, such as rising electrical resistance, decreasing sound velocity, specific heat peaks, internal friction peaks, etc. These phenomena may be attributed to the premartensitic transformation (6-15).

The premartensitic transformation of TiNi is suspected to be associated with a lattice modulation, due to periodic displacement of atoms. This lattice modulation can lower the energy of the materials and probably is electronic in origin. The formation of a charge density wave (CDW) was proposed to explain the premartensitic transformation behaviors (6-12). "A charge density wave is a static modulation of the conduction electrons, which is a Fermi-surface-driven phenomenon usually accompanied by a periodic lattice distortion." (6) " A favorable Fermi surface geometry is required for the formation of a CDW. A CDW will most likely occur when the shape of the Fermi surface can be connected by the same wave-vector Q., i.e. Q = 2Kf."(6) The presence of the CDW will alter the normal crystalline periodicity of the material because ion displacements appear to stabilize the charge perturbation. Because of the unlikelhood of favorable Fermi surface nesting, charge density waves are restricted in one- or two- dimensional materials. Though CDW phenomena are rarely found in three-dimensional materials, it is possible to find the formation of CDWs in the transition metals, due to their complex overlapping of d and f bands (6-12).

The wave vector of a CDW is not necessarily an integral fraction of a reciprocal lattice vector of the undistorted parent phase. The material exhibiting this phenomenon is in a quasi-crystalline phase called "incommensurate phase" (6).

A so-called "commensurate" or "locked-in" phase is the state when the wave vector of a CDW is exactly an integral fraction of its parent phase (7). Therefore, the formation of a CDW can be accompanied by two structural phase transformations which are the formations of incommensurate and commensurate phases.

The superlattice resulting from the formation of a CDW will create some satellite diffractions near the Bragg diffractions of the parent lattice (6-17). In TiNi alloys, the 1/3 position reflections are the results of the superlattice arising from a CDW.

When TiNi is cooled from its high temperature B2 parent phase, the first premartensitic transformation, which is second order, will start at Tp temperature, where the electrical resistance begins to increase and the structure has changed to distorted B2 incommensurate phase. Some diffuse streaks and extra diffraction spots can be found among the B2 diffraction pattern. The accompanying microstructural change gave rise to the separate antiphase domains can be found in the parent matrix (6-14).

With further cooling the incommensurate phase will change to commensurate phase at Td temperature, which is at the reflection point of the resistance curve between Tp and martensite start (Ms) temperatures. This is called the second premartensitic transformation which is first order. The structure will change from distorted B2 to rhombohedral R phase, while extra diffraction spots appear at exact 1/3 positions of rhombohedral diffraction pattern. At this stage, needle-like domains can be found associated with the second premartensitic transformation in the matrix.

Martensitic transformation starts with the abrupt decrease of electrical resistance due to the formation of martensite plates. R phases can coexist with martensite plates until Mf, martensite finish, temperature is reached. The crystal structure of martensite plates is distorted monoclinic B19'. The sequence of martensitic transformation can be described as follows : parent phase (B2)--- incommensurate phase (distorted cubic)--- commensurate phase (rhombohedral)---martensitic phase (monoclinic, B19') (6-8, 13,14,17).

Upon heating, austenite starts to form at As temperature, which is associated with an abrupt increase of electrical resistance. As the resistance begins to decrease, the austenite finish temperature (Af) is achieved. At this time, the structure has returned to its high temperature parent phase.

There are several factors affecting the martensitic transformation behavior of TiNi alloys, including alloy composition, thermal cycling, aging temperature, aging time, cooling rate, cold work, annealing after cold work, etc.

The transformation behaviors of TiNi alloys are very sensitive to the relative concentration of Ti and Ni

(10,18). The more Ni in the alloy, the lower the Ms temperatures is. The precipitate styles formed during aging treatments are controlled by composition of alloys (18). At least two types of precipitate have been found, i.e. Ti2Ni and TiNi3. The former appears in Ti rich alloys and the latter in Ni rich alloys. The formation of precipitates will change the matrix composition, which could raise or lower the Ms temperature, according to which type of precipitate is formed. The alloy used in this study is Ni rich; therefore, the formation of precipitate TiNi3 during aging treatments will decrease the concentration of Ni in the matrix. Thus, Ms temperature becomes higher. Alloying elements such as Cr, Cu, Fe and Al can trap vacancies in the alloy and therefore lower the Ms temperature (6-8, 10). The effects of composition and alloying elements are not studied in this research.

The increase of thermal cycling can suppress the Ms temperature to a different extent according to the thermomechanical history of the different specimens (19,20). In this study, the As-quenched specimen had a 10° C difference in Ms temperature after 90 thermal cycles from $+60^{\circ}$ C to -196°C, while 400°C-10hrs-water had only 2° C during the same thermal cycling. The dislocations introduced during thermal cycling impede the martensite formation, consequently depressing the Ms temperature. The effect arising from dislocations can be partially or almost totally eliminated by the formation of precipitates, which may obstruct the mobility of dislocations.

The effects of aging temperature can be separated into two groups, i.e. higher temperature aging and lower temperature aging. In this study, if the aging temperatures are higher than or equal to 600° C, the resulted electrical resistances will be very similar to that the of As-quenched specimen. The effect of aging at this temperature range is to shift the electrical hystereses towards higher temperature. When the specimens are aged at 500° C or lower, the formation of precipitates will lower the Ni concentration in the matrix, thus raising the Ms temperatures. If the size of the precipitates is too small, the coherency of precipitates and matrix will obstruct the martensite formation. This was the case with the specimen aged at 300° C for 1 hour and quenched into water.

The effect of aging time is evaluated by aging specimens at 400° C and 500° C for 1 hour to 10 hours. When aging time extends from 1 to 4 hours, the precipitates in the matrix will grow larger and consume more Ni from the matrix. This phenomenon will raise the Ms temperature and change the shape of the electrical resistance curve. Further aging from 4 to 10 hours has no apparent evident effect on either transition temperatures or shape of the electrical resistance curve. The equilibrium condition created between precipitates and matrix prohibits the further growth of precipitates. Therefore, the effects of aging for longer time periods are not obvious.

The effects of cooling rate on TiNi alloys may be divided into two groups. When the specimen is aged at higher temperatures, the slow cooling rate will introduce the opportunity of lower temperature aging. Though this lower temperature aging time is very short, a certain amount of precipitate can form. Since the aging time period is only seconds long, the precipitates aggregate along the grain boundaries in order to lower their nucleation energy. This phenomenon could probably be responsible for the depression of electrical resistance hysteresis.

When aged at lower temperatures, precipitates have already formed in the matrix and there is no difference in transition temperatures and electrical resistance curves between air-cooled and water-quenched specimens.

After the specimen was cold rolled, dislocations were introduced. The Ms temperature is depressed by the large quantity of dislocations which partially or completely prevent the stable reorientation or the growth of the martensite plates. These dislocations also affect the mobility of other dislocations which are responsible for the plastic flow. Many strain-induced martensite plates are formed in the matrix (16,17 19,21-23). These martensite plates are not thought to be mobile because of dense dislocations around them. In TEM observations, B2 diffraction pattern with diffuse streaks, extra 1/3 position diffraction spots and diffraction spots arising from martensite plates can be found in the same specimen. This represents the coexistence of parent phase, R phase and martensite phase. It is suspected that the R phases could probably nucleate preferentially on dislocations to lower their nucleation energy.

The effect of annealing on cold-rolled specimens is enormous (24), no matter what the degree of mechanical deformation. Annealing will dramatically change the transition temperatures and the shape of electrical resistance vs. temperature curves by creating a dislocation substructure. This substructure can obstruct the growth of martensite plates, but makes the reorientation of these plates easier. This may lead to the formation of microtwins, which are suspected of being responsible for the pseudoelasticity below Ms temperature.

Since the surprising similarity of transition temperatures and electrical resistance vs. temperature curves between "cold-rolled and annealed" specimens and specimens aged at same temperature, it may be concluded that the effect of the formation of precipitates is larger than that of the introduction of dislocations.

In this study, all the factors described above, except alloy composition, are combined to investigate the effect of thermomechanical treatments on the transformation behaviors of a TiNi alloy. It is concluded that the formation of precipitates and the introduction of dislocations are two controlling factors affecting martensitic, as well as premartensitic, transformations.

II. EXPERIMENTAL PROCEDURES

A Ti-51.7Ni (at. pct.) alloy was used for this study. The bulk material was a 2cm x 2cm x 10cm bar, which was cut into 50.0mm x 2.0mm x 0.3mm strips for electrical resistance tests. The strips were sealed in quartz tubes under vacuum condition and were annealed at 900°C for 1 hour followed by quenching into water by breaking the tubes. These annealed specimens were denoted by "As-quenched" for convenience. In this study, all the annealing and aging heat treatments were performed while the specimens were sealed in quartz tubes under vacuum condition. The aged specimens were aged at different temperatures, ranging from 300°C to 900°C for 1 hr to 10 hrs. The effect of cooling rate on TiNi was evaluated by observing the two different rates obtained by water quenching and air cooling, after specimens had been aged. The aged specimens were denoted by their aging temperatures, aging time and cooling rate such as 900°C-1hr-air and 400°C-10hrs-water, etc (See Table 1).

The cold-rolled specimens for electrical resistance tests were cut into 0.5mm thick strips, following the same heat treatment as that for As-quenched specimens. These 0.5 mm thick strips were rolled at ambient temperature to 40%, 20% and 10% reduction in thickness, and they are denoted as

C-R-40%, C-R-20% and C-R-10%, respectively. These cold-rolled specimens were then mechanically polished to standard size, i.e., 50.0mm x 2.0mm x 0.3mm. The "cold-rolled and annealed" specimens were made following the same procedures as cold-rolled specimens and then were annealed at 500° C for 1 hour and quenched into water. These specimens, corresponding to 40%, 20% and 10% reduction in thickness, were denoted by C-R-40%--500° C-1hr-water, C-R-20%--500° C-1hr-water and C-R-10%--500° C-1hr-water, respectively (See Table 2).

Before electrical resistance tests, all the specimens were electropolished in electrolyte consisting of 8% perchloric acid and 92% glacial acetic acid (by volume) by applying 25 volts in order to get rid of the oxidized layer on sample surface caused by heat treatments.

The electrical resistance tests were caried out from +60° C to -196° C by using an Omnigraphic 200 X-Y recorder. The electrical resistance vs. temperature curves were automatically recorded. The controlling of temperature while cooling was performed by immersing the specimens into or withdrawing them out of a deep, wide-mouth container holding liquid nitrogen. A rate of 3.3cm/minute was maintained using a Hurst stepping motor. For heating, the specimens were put in an 11 ohm resistor coil set in a stable air condition and 30 volts in direct current were applied with the stepping motor shut off.

A copper-constantan thermocouple was spot-welded to the centers of the specimens while four copper wires were also spot- welded to the ends. The outer two copper wires were connected to the d.c. power supply which was a current source, and the inner two were connected to the X-Y 200 recorder. The d.c. power supply applied 140 V to the specimens, with a 1000 ohm resistor producing a current of 140 mA.

The TEM specimens were cut from the bulk material into strips with thickness 0.25mm and 0.5mm for non-rolled and rolled specimens respectively. The same thermomechnical treatments as performed on the corresponding electrical resistance specimens were performed on these strips. They were then mechanically polished and cut into small discs, with 3mm in diameter and 0.15mm thick. The reason for using thick strips to prepare TEM specimens was to avoid surface artifacts probably caused by contamination from oxygen and/or nitrogen diffusion during heat treatments (25). Jet polishing was carried out at room temperature in a Struers Tenupol II by using 8% perchloric acid and 92% glacial acetic acid (by volume) as electrolyte while applying 20 volts d.c. The TEM observations were conducted in a Hitachi H-800 Transmission Electron Microscope operating at 200 KV at room temperature, i.e., apprroximately 20°C .

III. RESULTS AND DISCUSSION

All of the transition temperatures obtained from electrical resistance tests of the aged specimens and cold rolled specimens, including Ms, Mf, As, Af,Tp and Td temperatures, are summarized in Table 1 and Table 2 respectively. In this study several variables were changed in order to determine their effects on premartensitic as well as martensitic transformations. These variables include : aging temperature, aging time, cooling rate, degree of deformation (i.e., thickness reduction percentage in cold rolling) and thermal cycling. Finally, the effect of annealing following cold rolling was also examined.

A) As-quenched specimen

The As-quenched specimen was annealed at 900° C for 1 hr and then quenched into water without any further thermomechanical treatments. The electrical resistance vs. temperature curve of the As-quenched specimen for the first thermal cycle between +60° C and -196° C is plotted in Fig. 1(a).

When this As-quenched specimen is cooled down from +60° C, the electrical resistance starts to rise at Tp (+30° C), while the first premartensitic transformation begins and

Table 1. Transition temperatures of annealed and aged specimens

Specimen	Ms	Mf	As	Af	Tp	Td (°C)
900° C-1hr-water	-94	<-196	-82	-52	+30	-70
900° C-1hr-air	-134	<-196	<-196	-196	+25	-67
800° C-1hr-water	-104	<-196	-77	-53	+22	-80
700° C-ihr-water	-96	<-196	-86	-51	+24	-67
600° C-1hr-water	-87	<-196	-75	-43	+25	-64
600° C-4hrs-water	-66	-110	-56	-31	+20	+56
500° C-1hr-water	-44	<-196	+2	+15	+40	+18
500° C-4hrs-water	-13	-8	+17	+26	+33	+20
500° C-10hrs-water	-14	-49	+22	+26	+30	+20
400° C-1hr-water	-38	<-196	<-196	-27	+49	+28
400° C-4hrs-water	-26	<-196	+3	+11	+52	+35
400° C-10hrs-water	-22	<-196	+8	+21	+54	+36
400° C-1hr-air	-40	<-196	-26	-12	+54	+25
300° C-1hr-	-125	<-196	<-196	-125	+14	-34

Table 2. Transition temperatures of cold-rolled and "cold-rolled and annealed" specimens

Specimen	Ms	Mf	As	Af	Tp	Td (°C)
C-R-10%	-130	<-196	<-196	-160	---	---
C-R-20%	-130	<-196	<-196	-155	---	---
C-R-40%	-164	<-196	<-196	-164	---	---
C-R-10%-500° C-1hr-water	-38	<-196	+2	+15	+38	+18
C-R-20%-500° C-1hr-water	-42	<-196	-2	+16	+40	+19
C-R-40%-500° C-1hr-water	-44	<-196	-18	+10	+41	+19

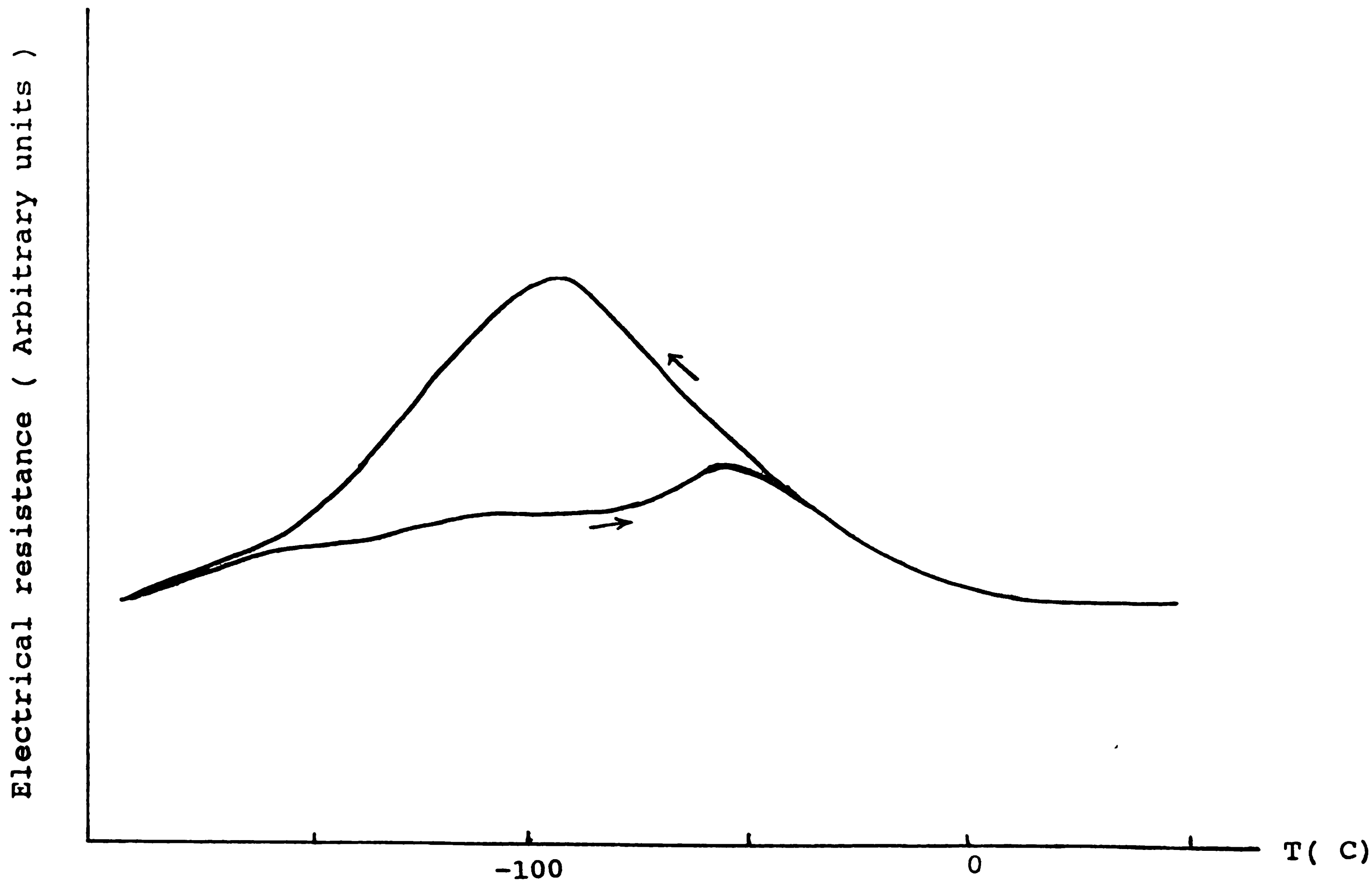

Fig. 1(a). Electrical resistance vs. temperature curve of thermal cycle 1 between +60° C and -196° C, As-quenched specimen.

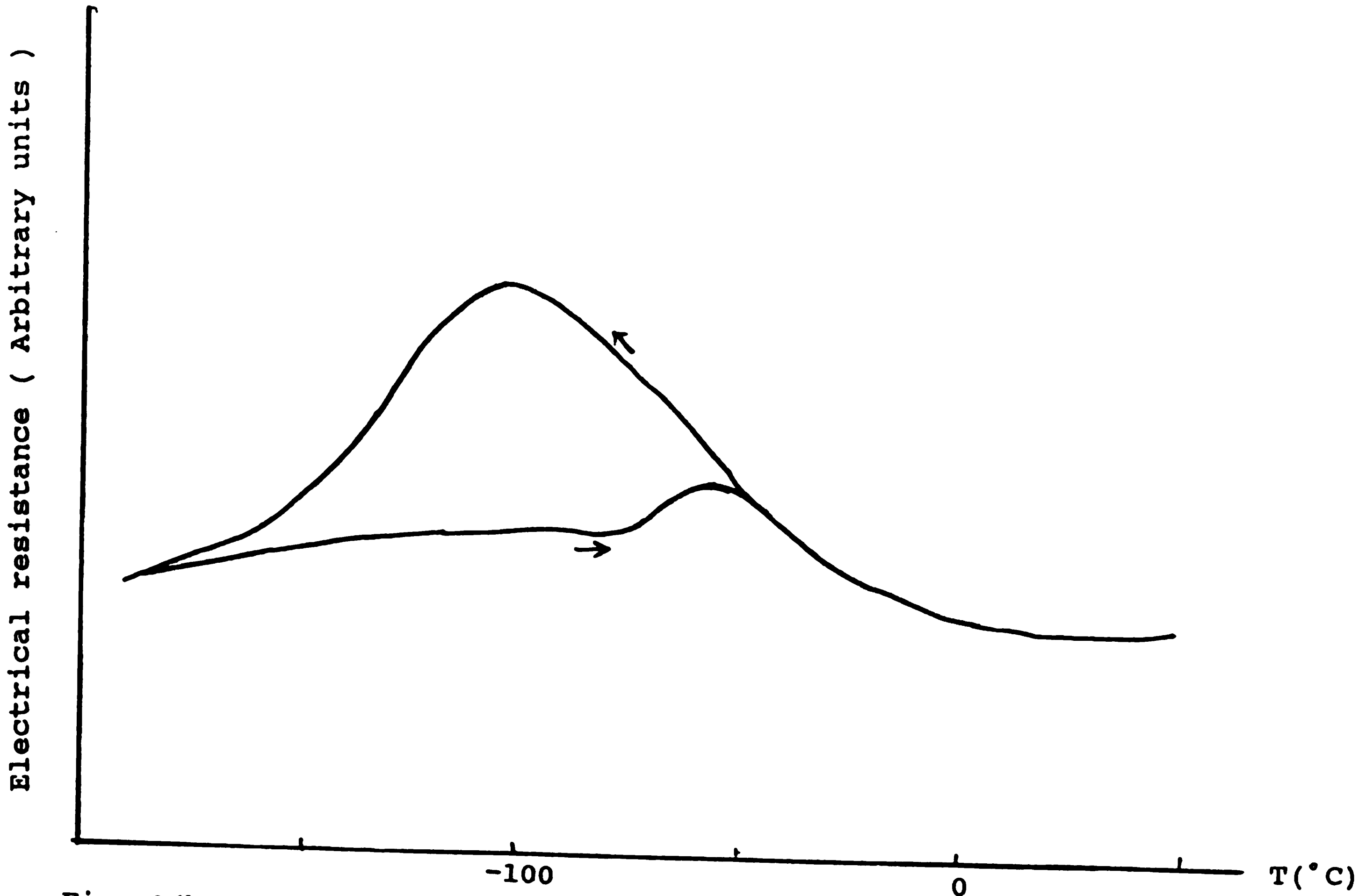

Fig. 1(b). Electrical resistance vs. temperature curve of thermal cycle 90 between +60° C and -196°C, As-quenched specimen.

the B2 parent phase transforms to incommensurate phase (distorted B2). Fig. 2(a) is the bright field image of this incommensurate phase. No microstructure other than extinction contour has been observed. The selected area diffraction patterns from the same specimen are shown in Figs. 2(b), 2(c) and 2(d), identified as <111>B2, <110>B2 and <210>B2, respectively. In addition to the exact Bragg diffraction positions from the B2 parent phase, diffuse streaks appear around 1/3 positions of the B2 reciprocal lattice. Since these streaks, arising from the incommensurate phase, are too faint and too diffuse to be indexed, they will be indexed by using different specimens.

The second premartensitic transformation starts at Td (-70° C) which is determined as the inflection point of the resistance curve between Tp and Ms temperatures. Because Td is much lower than room temperature, the first premartensitic transformation observed under TEM is not obvious. This phenomenon is suspected of being responsible for the vagueness of the extra spots at 1/3 B2 diffraction patterns. Below Td temperature, the commensurate phase, denoted by R phase, has been determined to have rhombohedral structure. The corresponding extra diffraction spots at 1/3 positions of the B2 reciprocal lattice from R phase can be seen in differently heat-treated specimens at room temperature. Martensitic transformation starts at Ms (-94° C), where the

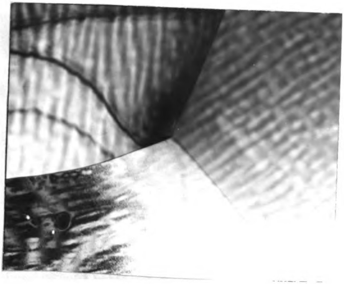

2(a)

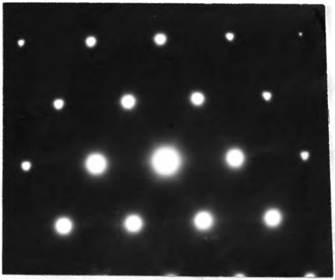

2(b)

Fig. 2(a) to 2(d). Transition electron micrograph and diffraction patterns of As-qienched specimen.
2(a) Bright field micrograph, mag.50,000x
2(b) [111] B2 zone diffraction pattern

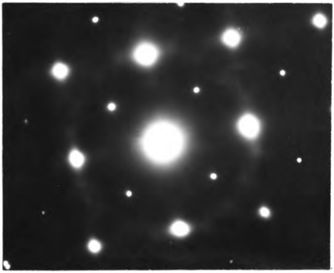

2(c)

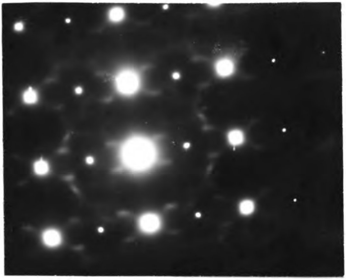

2(d)

2 (c) [110] B2 zone diffraction
2 (d) [210] B2 zone diffraction

resistance begins to decrease abruptly. Mf is reached when all the R phases transform into martensite. The Mf of As-quenched specimen is very colse to or slightly lower than liquid nitrogen temperature. The martensite structure has already been determined as distorted monoclinic (B19') structure with the lattice parameter a = 28.89nm, b = 41.20nm, c = 46.22nm and β = 96.80°. Upon heating, austenite start temperature As (-82° C) is reached at the point of the abrupt increase in the resistance curve, and austenite finish temperature Af (-52° C) at the point of sharp decrease in resistance. Between cooling and heating curves, there exists a large electrical resistance hysterisis. After reaching Af temperature the specimen has returned to its parent phase.

B) Effect of aging temperature

The effect of aging temperature on TiNi was studied by keeping other variables constant. The condition chosen was aging specimens at temperatures ranging from 300° C to 900° C for 1 hour, followed by water quenching. Figs. 3 through Fig. 8 are the electrical resistance vs. temperature curves for specimens aged at from 800° C to 300° C respectively. The transition temperatures from the firt cycle of the aged specimens are summarized in Table 1, including Ms, Mf, As, Af, Tp and Td etc, while they are compared in Fig. 9. For specimens aged from 800° C to 400° C, the lower the aging temperatures, the higher the Ms, Tp and Td are. The shapes of the resistance curves of 800° C-1hr-water, 700° C-1hr-water and 600° C-1hr-water are very similar to that of the As-quenched specimen. The aging effect within this temperature range is the shifting of the resistance curves towards higher temperatures.

The resistance curve of 500° C-1hr-water is different from those of specimens aged at higher temperatures. Precipitates are formed in the matrix with the size of 70° nm x 17nm. The formation of precipitates will lower the concentration of Ni in the matrix which could cause the increase of Ms temperature. The bright field and dark field micrographs of precipitates associated with its selected area diffraction micrograph are shown in Figs. 6(b), 6(c) and 6(d) respectively. Since Td is very close to room temperature (Td = +18°C), the matrix is in R phase which has rhombohedral structure. The composition of these precipitates is reported as about TiNi3, having hexagonal structure. There were three variants of precipitates with different orientations, and their longititudinal directions of precipitates have been determined (See Fig. 6(d)). The morphology of these cigar-like precipitates can be confirmed by the fringes at the edges of each grain.

The resistance curve of 400° C-1hr-water is very special due to its heating curve. No obvious As can

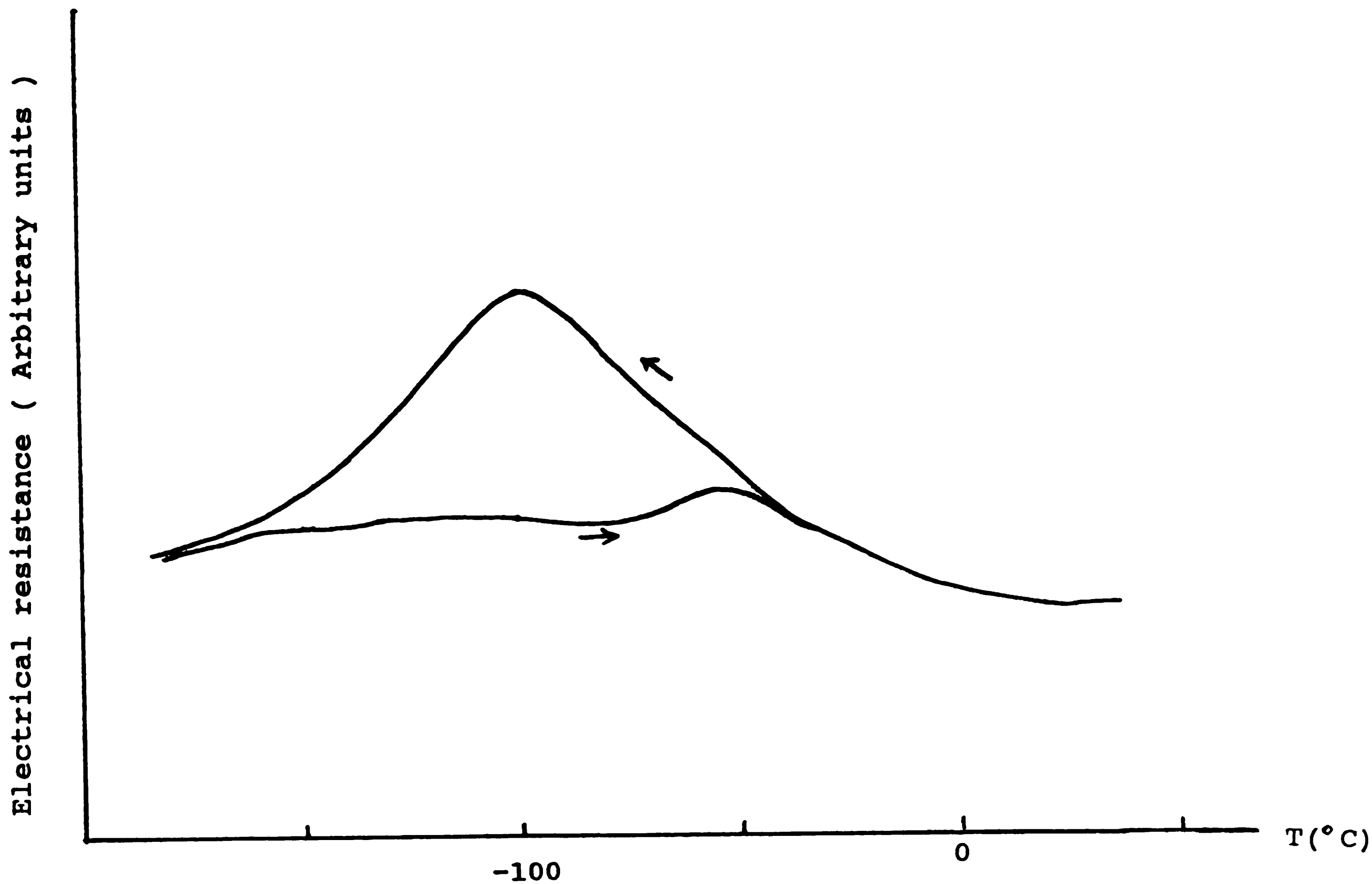

Fig. 3. Electrical resistance vs. temperature curve of thermal cycle 1 between +60° C and -196° C, specimen 800° C-1hr-water.

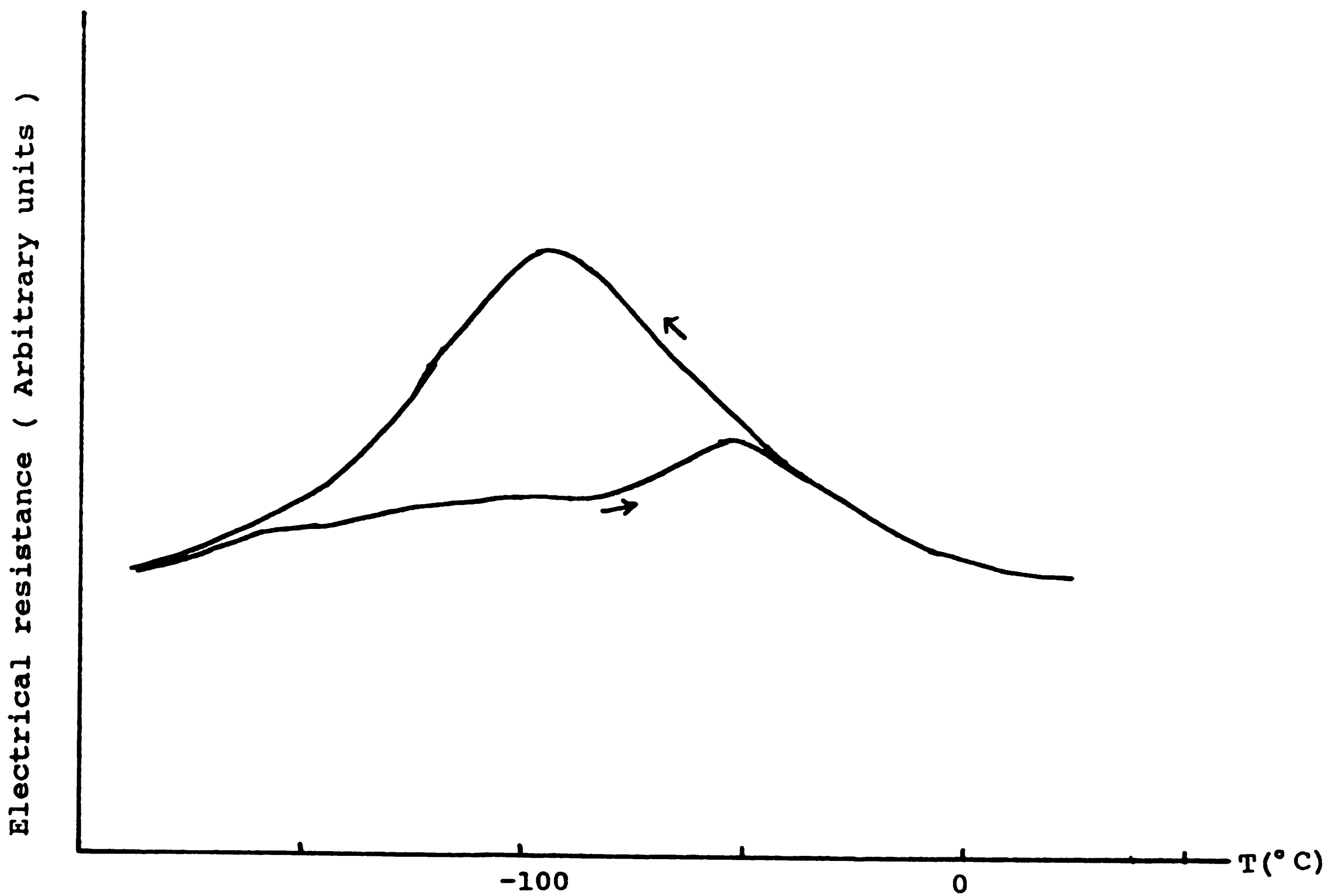

Fig. 4. Electrical resistance vs. temperature curve of thermal cycle 1 between +60° C and -196° C, specimen 700° C-1hr-water.

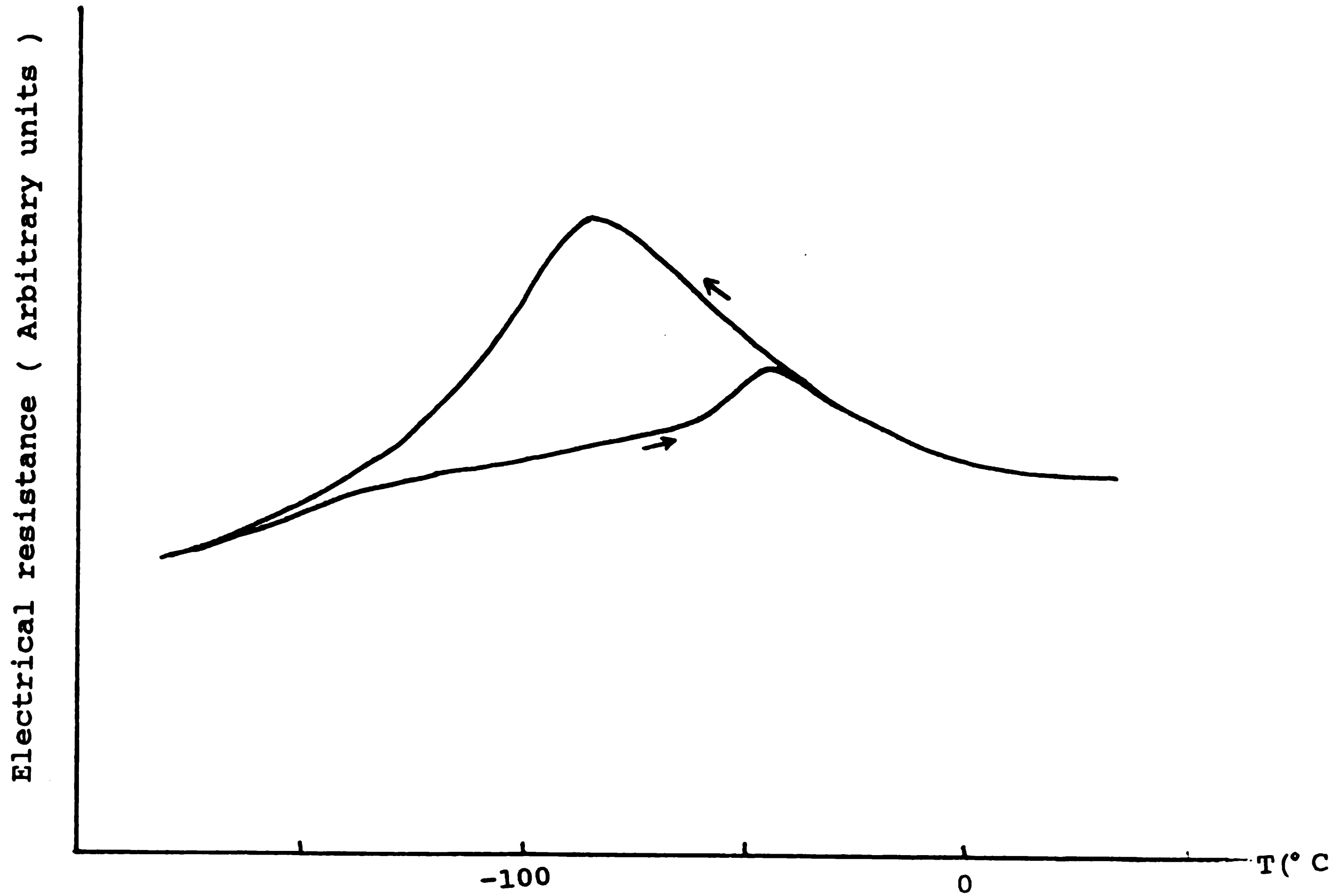

Fig. 5. Electrical resistance vs. temperature curve of thermal cycle 1 between +60° C and -196° C, specimen 600° C-1hr-water.

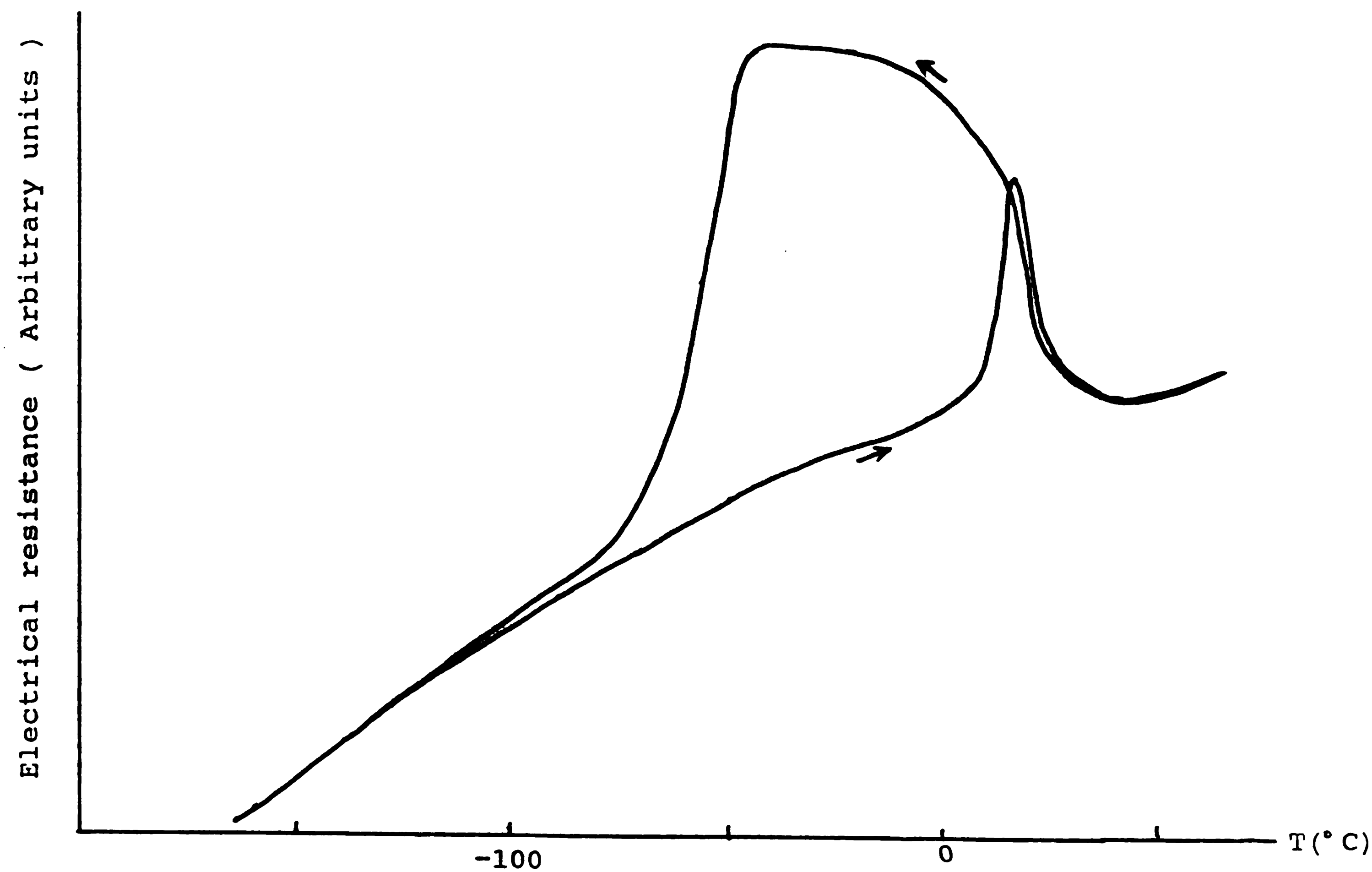

Fig. 6(a). Electrical resistance vs. temperature curve of thermal cycle 1 between +60°C and -196°C, specimen 500°C-1hr-water.

6(b)

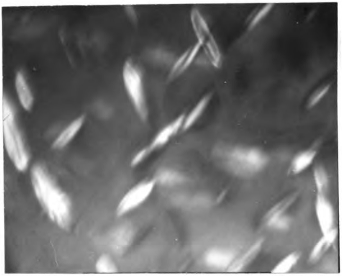

6(c)

Figs. 6(b) to 6(d). Transmission electron micrographs and selected area diffraction pattern of specimen 500° C-1hr-water
6(b) Bright field micrograph, mag. 300,000X
6(c) Dark field micrograph. mag. 300,000X

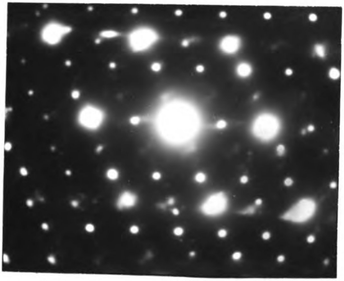

6(d)

6(d) Diffraction pattern contains spots from parent phase and precipitates.

be found and the hysterisis is extremely small. Since Td is above room temperature, the specimen is in commensurate phase and the corresponding R phase appears. The formation of precipitates raises the Ms temperature. The extra 1/3 position reflections arising from superlattice of parent phase is strong enough to be indexed (See Fig. 7(c)). The size of precipitates of 400 C-1hr-water, 13nm x 6nm, is much smaller than that of 500^{o} C-1hr-water precipitates. The Widmanstatten structure in precipitates indicates decomposition of the parent phase on aging. These precipitates seem to be coherent to the matrix. In Figs. 7(d),(e) and (f), the dark field micrograph, bright field micrograph and corresponding selected area diffraction pattern of one variant of the precipitates are shown. The expected needle-like domains have been observed in some areas but no fringes around its boundaries even tilting the specimen from $+60^{o}$ to -60^{o} . This phenomenon is different from the needle-like domains reported previously.

The electrical resistance vs. temperature curve of 300 C-1hr-water has been depressed so seriously that its resistance hysteresis at Ms is even lower than liquid nitrogen temperature. The hysteresis shown in Fig. 8. is the one corresponding to Td temperature. The precipitates formed in this specimen are so small that they maintain coherency with the matrix. This coherency might obstruct the formation of martensite thus lower the Ms

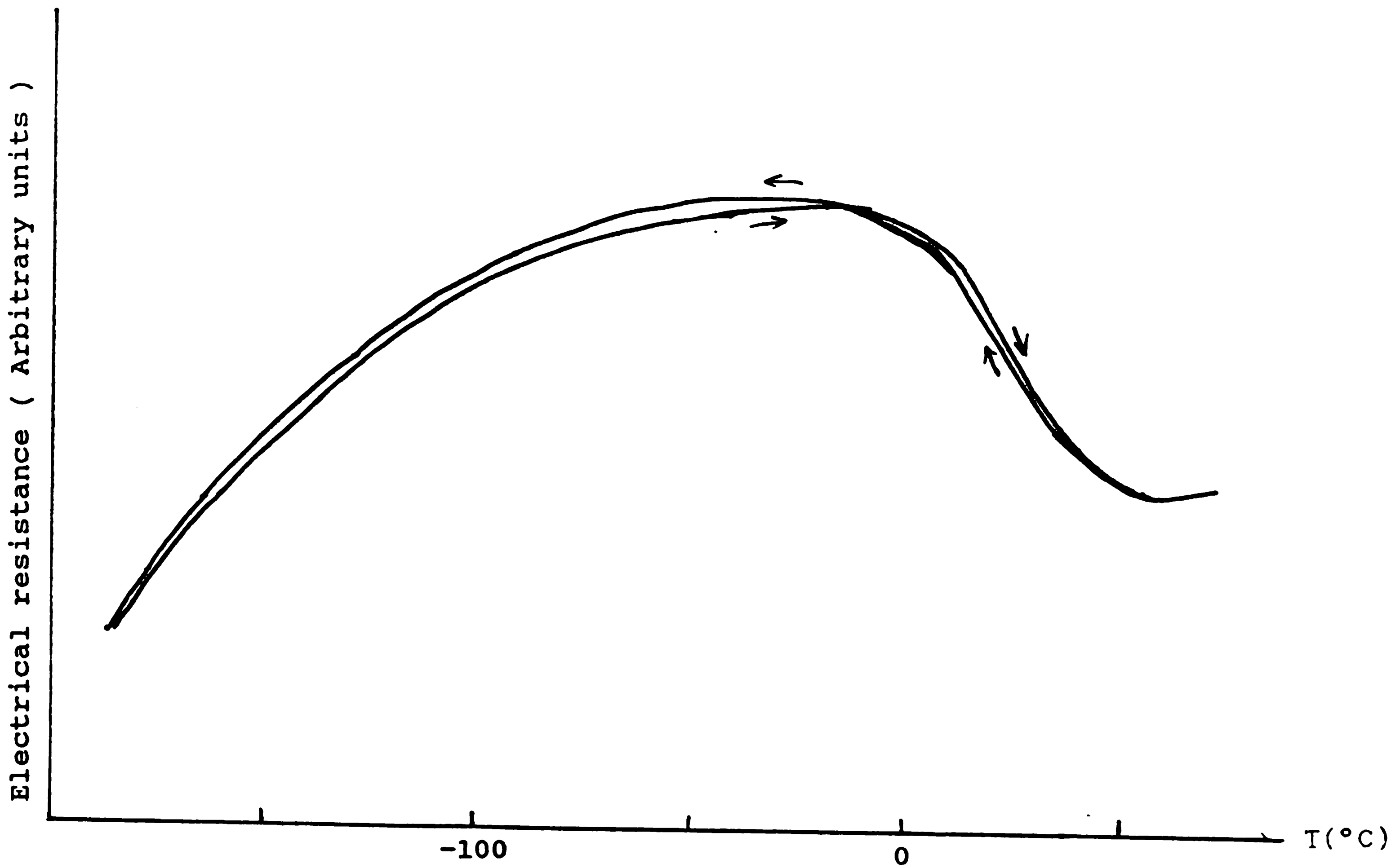

Fig. 7(a). Electrical resistance vs. temperature curve of thermal cycle 1 between +60° C and -196° C, specimen 400° C-1hr-water.

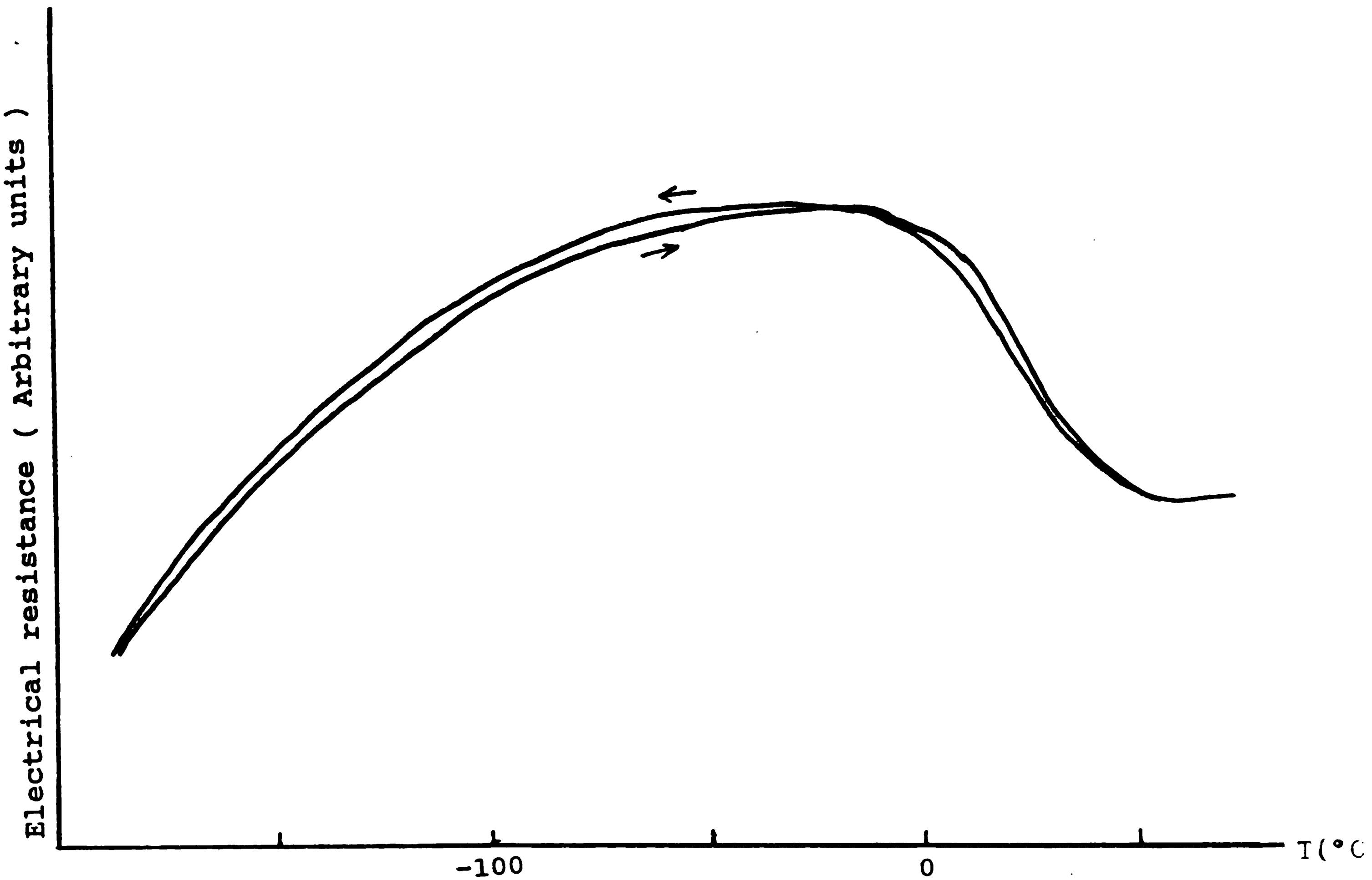

Fig. 7(b). Electrical resistance vs. temperature curve of thermal cycle 90 between +60°C and -196°C, specimen 400°C-1hr-water.

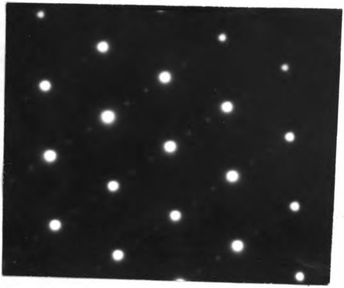

7(c)

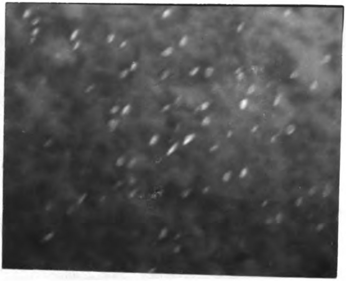

7(d)

Figs. 7(c) to 7(f). Transmission electron micrographs and selected area diffraction patterns of specimen 400° C-1hr-water.
7(c) [001]H diffraction with 1/3 (100) extra spots.
7(d) Dark field micrograph showing precipitates, mag. 300,000X

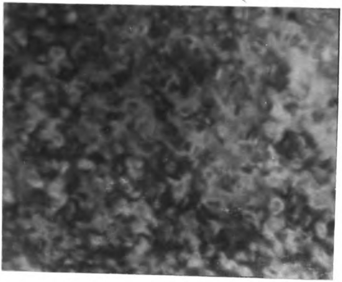

7(e)

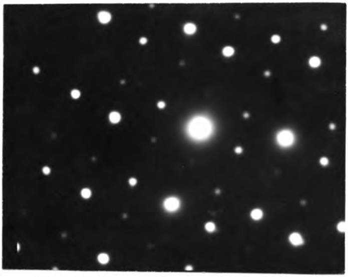

7(f)

7(e) Bright field micrograph, corresponding to 7(e)
7(f) Selected area diffraction corresponding to 7(d) and 7(e)

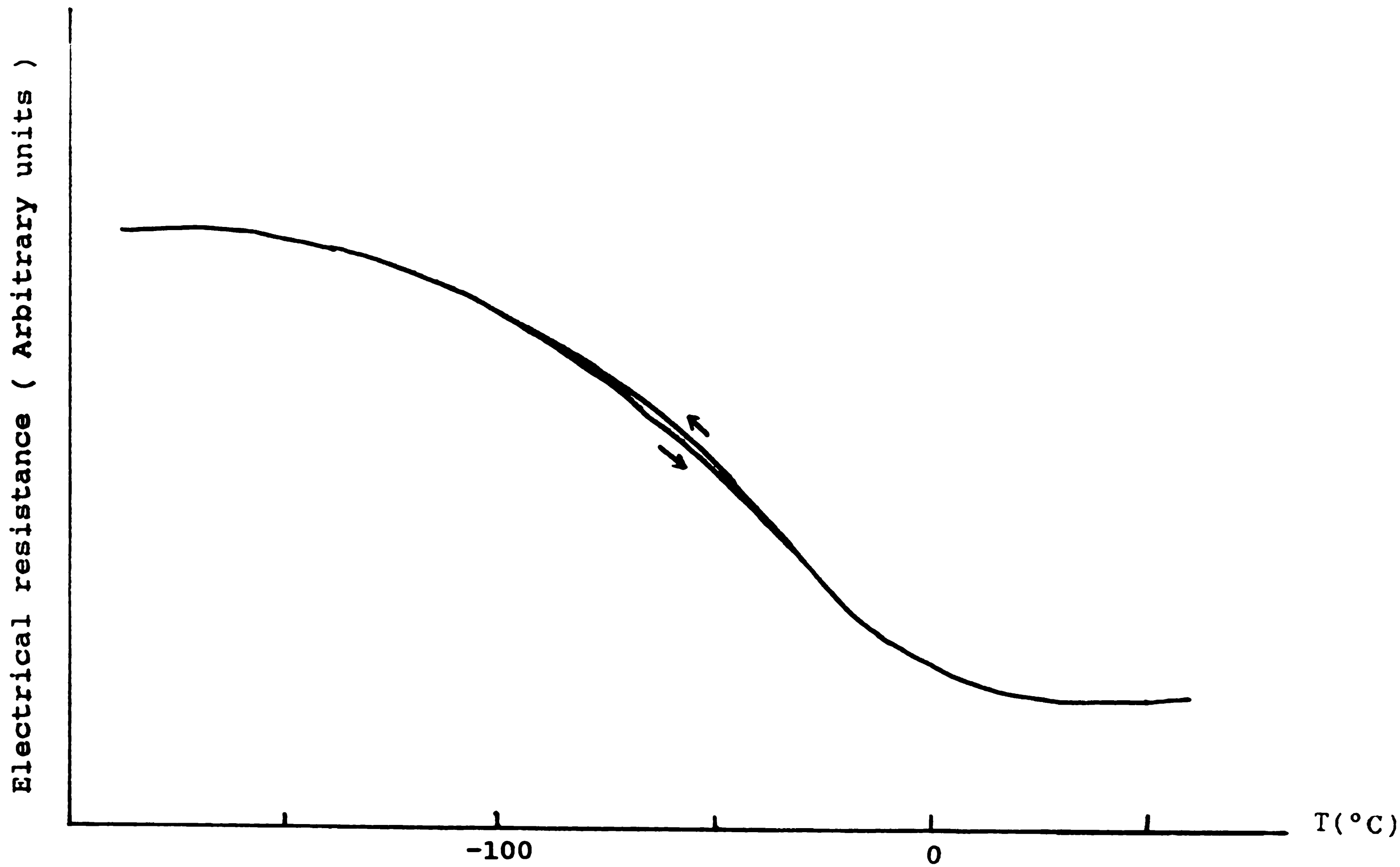

Fig. 8. Electrical resistance vs. temperature curve of thermal cycle 1 between +60° C and -196° C, specimen 300° C-1hr-water.

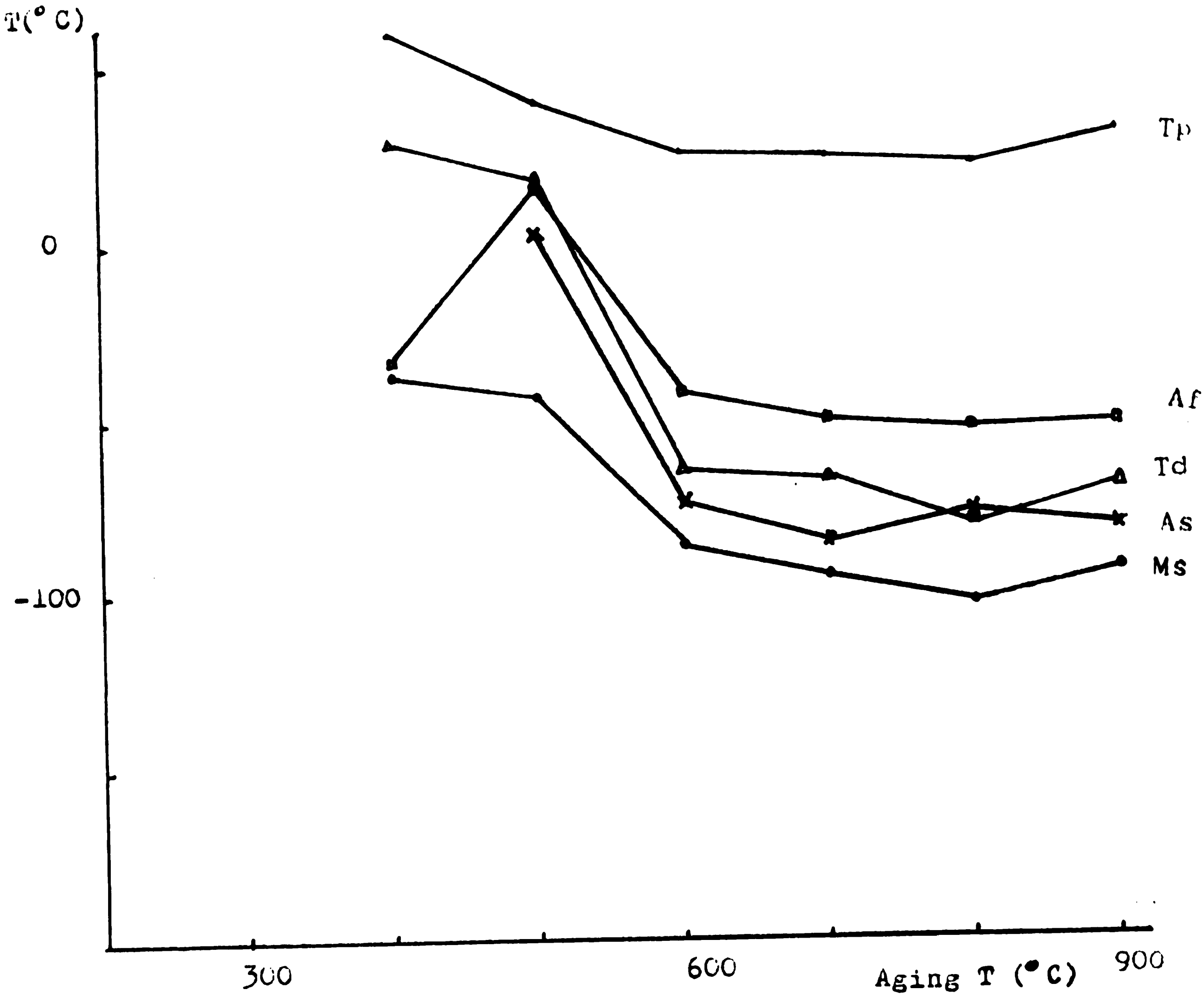

Fig. 9. Aging temperature effect on transition temperatures.

temperature.

C) Effect of aging time

Two aging temperatures, 400° C and 500° C, combined with three different aging time periods, 1hr, 4hrs and 10hrs, followed by water quenching were chosen to evalute the effect of aging time.

1) 500 C-X hrs-water

Specimen 500° C-1hr-water has been described previously. The electrical resistance vs. temperature curves of 500 C-4hrs-water and 500 C-10hrs-water are very much similar, as shown in Fig. 10 and Fig. 11(a) respectively, and are quite different from that of 500° C-1hr-water. The transition temperatures of these three specimens are compared in Fig. 12.

As the aging time is extended from 1 hour to 4 hours, the Ms, As and Af increase while Td is about the same and the resistance hysteresis is depressed and contracted, i.e., the resistance peak at Ms is lowered and the premartensitic transition zone narrowed. Meanwhile, the electrical resistance peak at Af of 500° C-4hrs-water and 500 C-10hrs-water is much lower than that of 500° C-1hr-water. There is no significant effect by further aging from 4 hrs to 10 hrs. In Fig. 11(b), the size of precipitates in 500° C-10hrs-water, 290 nm x 50nm, is much larger than those in 500° C-1hr-water. The formation of precipitates can lower the concentration of Ni in matrix, which will raise the Ms temperature. The bright field and dark field micrographs and corresponding selected area diffraction pattern are shown in Fig. 11(c), (d) and (e) respectively. At least three different precipitate variants have been observed. The morphology of these cigar-like precipitates can be confirmed by the existence of fringes near the boundaries of precipitates.

2) 400° C-X hrs-water

The hysteresis of electrical resistance vs. temperature curve of 400° C-1hr-water is very narrow from Tp to Ms where two hystereses exist. The reason for the formation of the first (smaller) hysteresis is still unknown, though the premartensitic transformation has been enhanced.

The electrical resistance vs. temperature curves of 400° C-4hrs-water and 400° C-10hrs-water are very similar to each other, as shown in Fig. 13 and Fig. 14(a) just as the specimens aged at 500° C. The resistance curves of specimens aged at times longer than 1 hour will have much larger hystereses between Ms and As, while the other (smaller) hystereses will appear between Tp and Af.

The aging effect on specimens aged more than 4 hours is not significant when comparing resistance curves of 400 C-4hrs-water and 400° C-10hrs-water. The premartensitic transformation is enhanced by longer (> 1 hr) aging

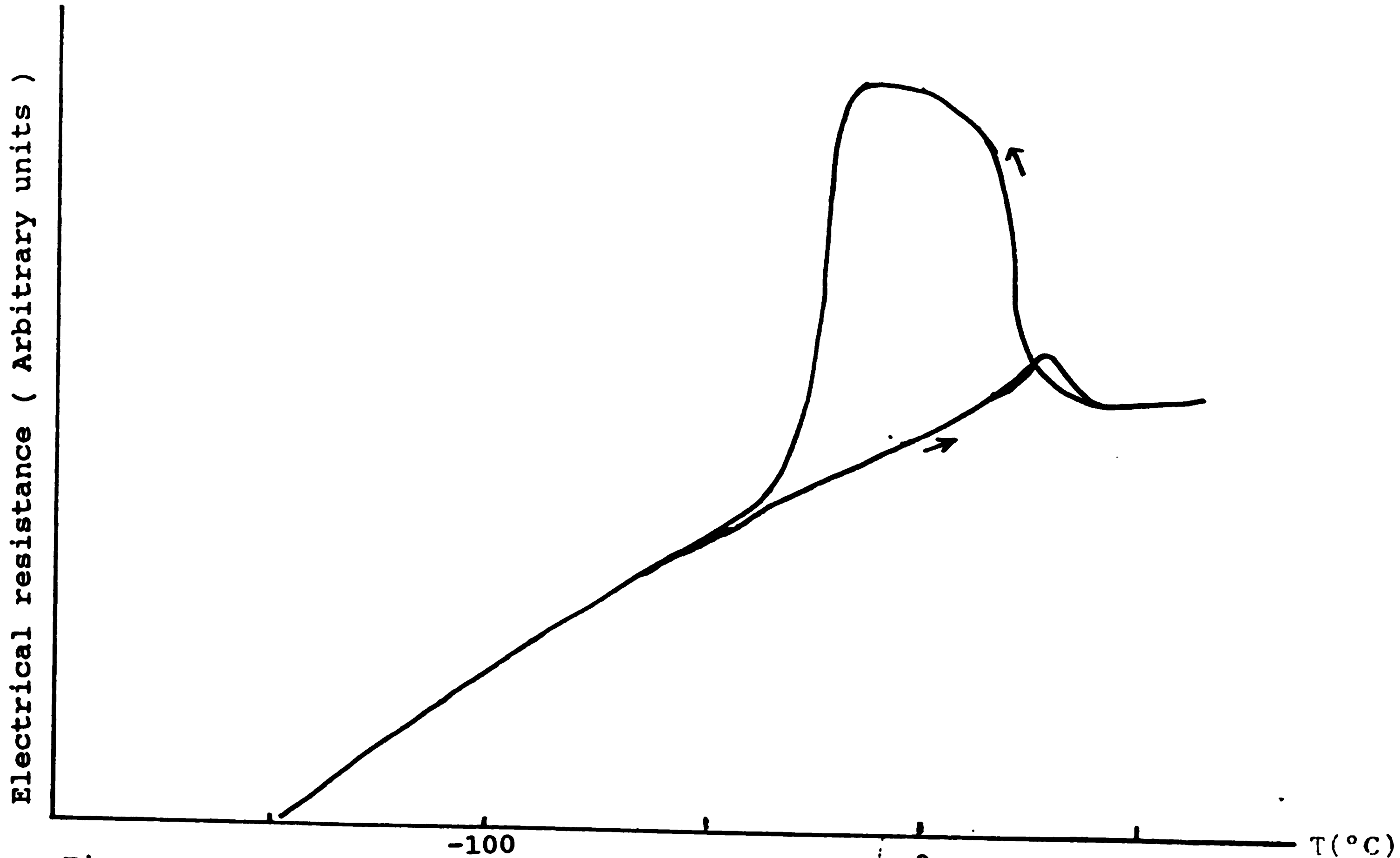

Fig. 10. Electrical resistance vs. temperature curve of thermal cycle 1 between +60° C and -196° C, specimen 500° C-4hrs-water.

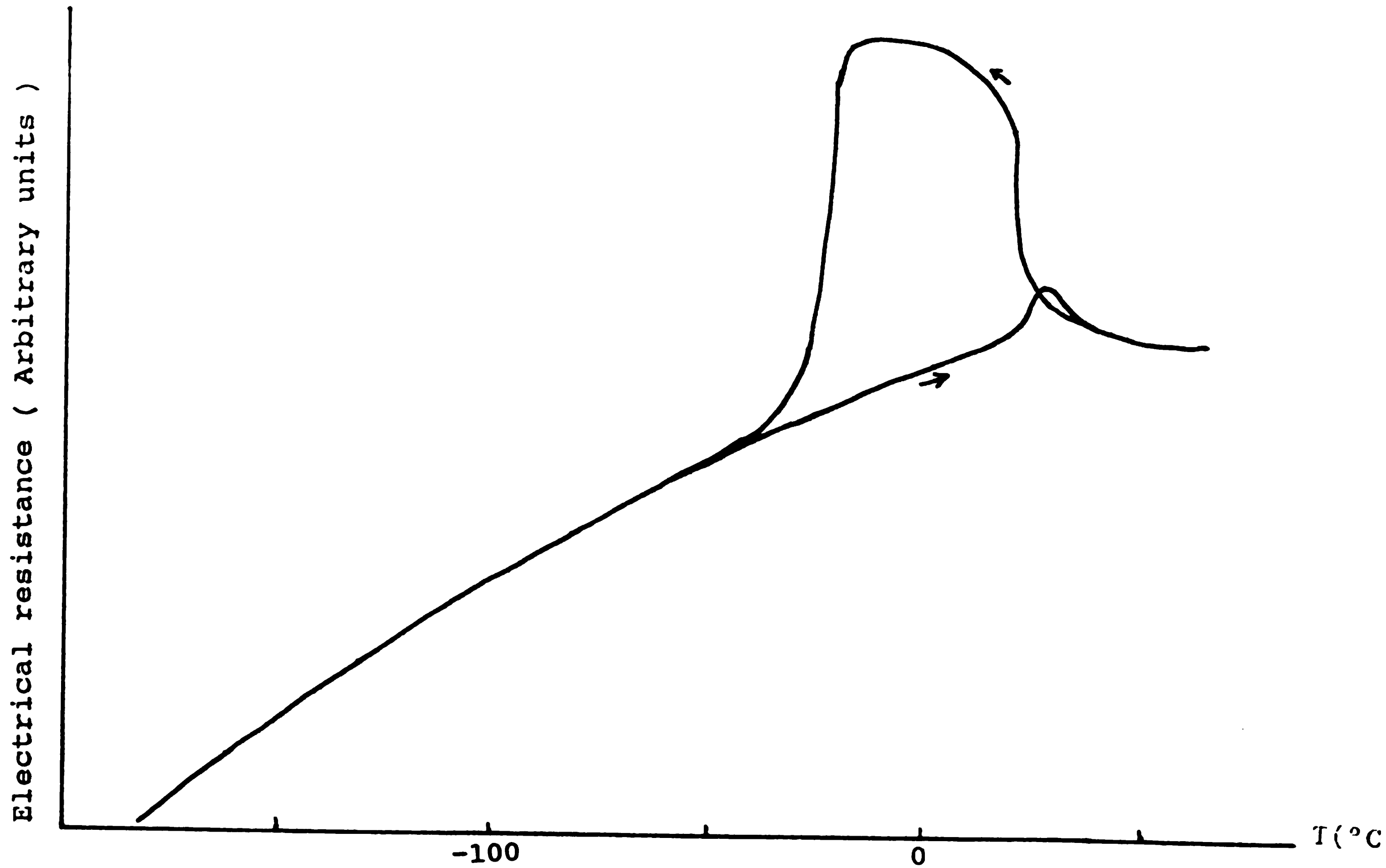

Fig. 11(a). Electrical resistance vs. temperature curve of thermal cycle 1 between +60° Cand -196° C, specimen 500° C-10hrs-water.

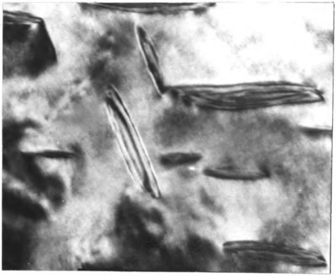

11(b)

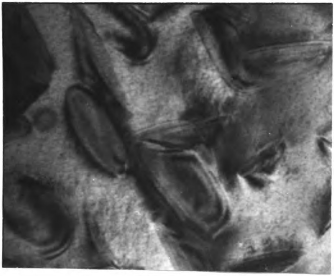

11(c)

Figs. 11(b) to 11(e). Transmission eletron micrographs and diffraction pattern of specimen 500° C-10hrs-water
11(b) Bright field micrograph showing precipitates, mag. 150,000x
11(c) Dark field micrograph of specimen 500° C-10hrs-water, mag. 200,000x

11(d)

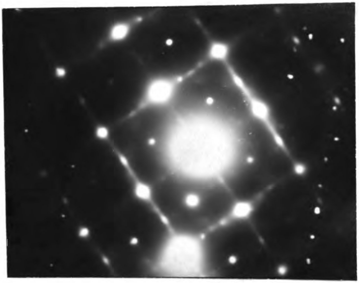

11(e)

11(d) Dark field micrograph of specimen 500° C-10hrs-water corresponding to 11(c), mag. 200,000x
11(e) Selected area diffraction pattern coresponding to 11(c) and 11(d)

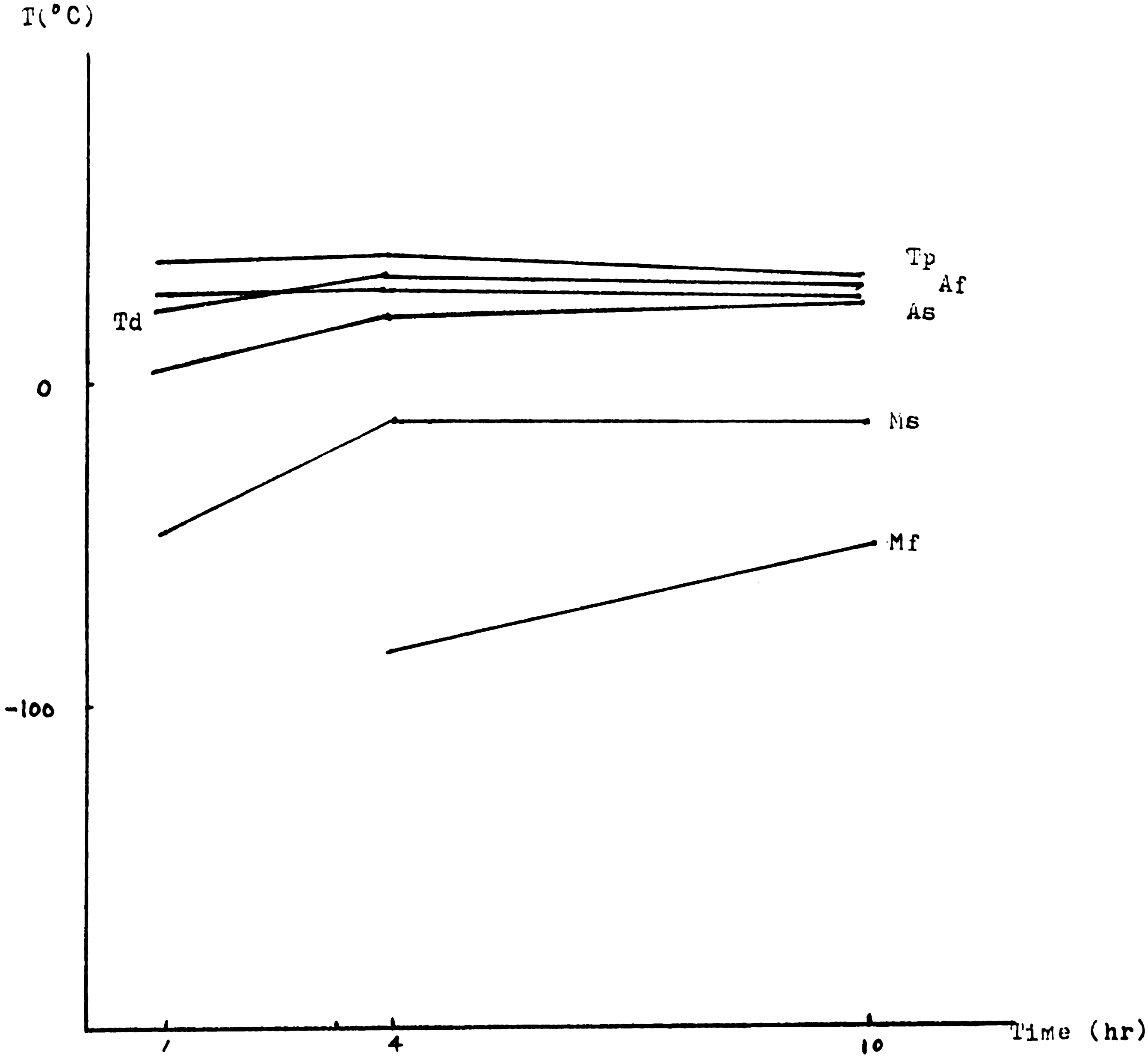

Fig. 12. Aging time effect on transition temperatures of specimens aged at 500° C.

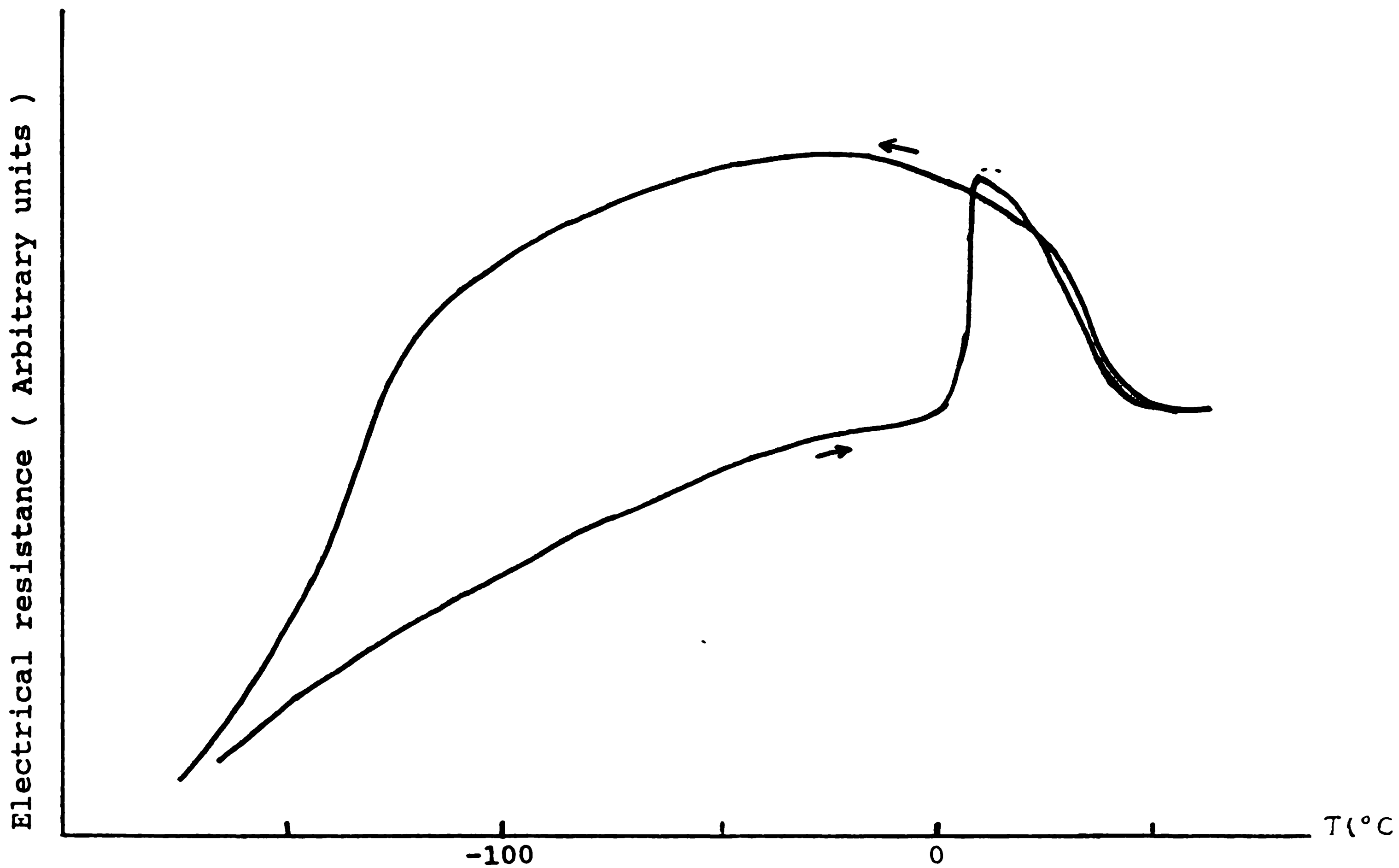

Fig. 13. Electrical resistance vs. temperature curve of thermal cycle 1 between +60° C and -196° C, specimen 400° C-4hrs-water.

heat treatments. It is suspected that the growth of precipitates decreases the Ni concentration in matrix which raises the Ms temperatures. Among all the specimens studied, 400 C-10hrs-water has the most pronounced premartensitic transformation and the 1/3 positions extra reflections are extremely clear. From Fig. 14(c) and (d), selected area diffraction patterns of different orientations are shown. Since the Td is higher than room temperature, R phase should dominate the whole specimen. The extra reflection spots are at exact 1/3 positions of matrix diffraction pattern. Again, suspected needle-like domains are found, but accompanied with no fringes along their boundaries (See Fig. 14 (e)). The diffraction spots arising from precipitates appearing in the selected area diffraction patterns are indicated in the figures. Figs. 14(f) to 14(h) show dark field and bright field micrographs and their corresponding diffraction patterns. Since six 1/3 position spots were included in the objective lens aperture due to the restriction of aperture size, the other 6 diffraction spots arising from precipitates were also included. The bright portion in dark field micrograph confirms the exitsence of precipitates, while the contrast for commensurate R phase is very poor.

It is natural to conclude that the effect of aging time is dominated by the formation and growth of precipitates. As the aging time exceeds a certain time

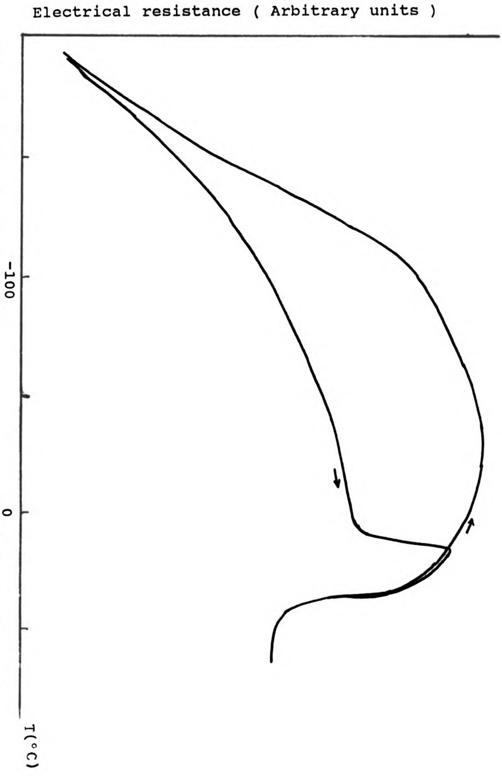

Fig. 14(a). Electrical resistance vs. tempertaure curve of thermal cycle 1 between +60° C and -196° C, specimen 400° C-10hrs-water.

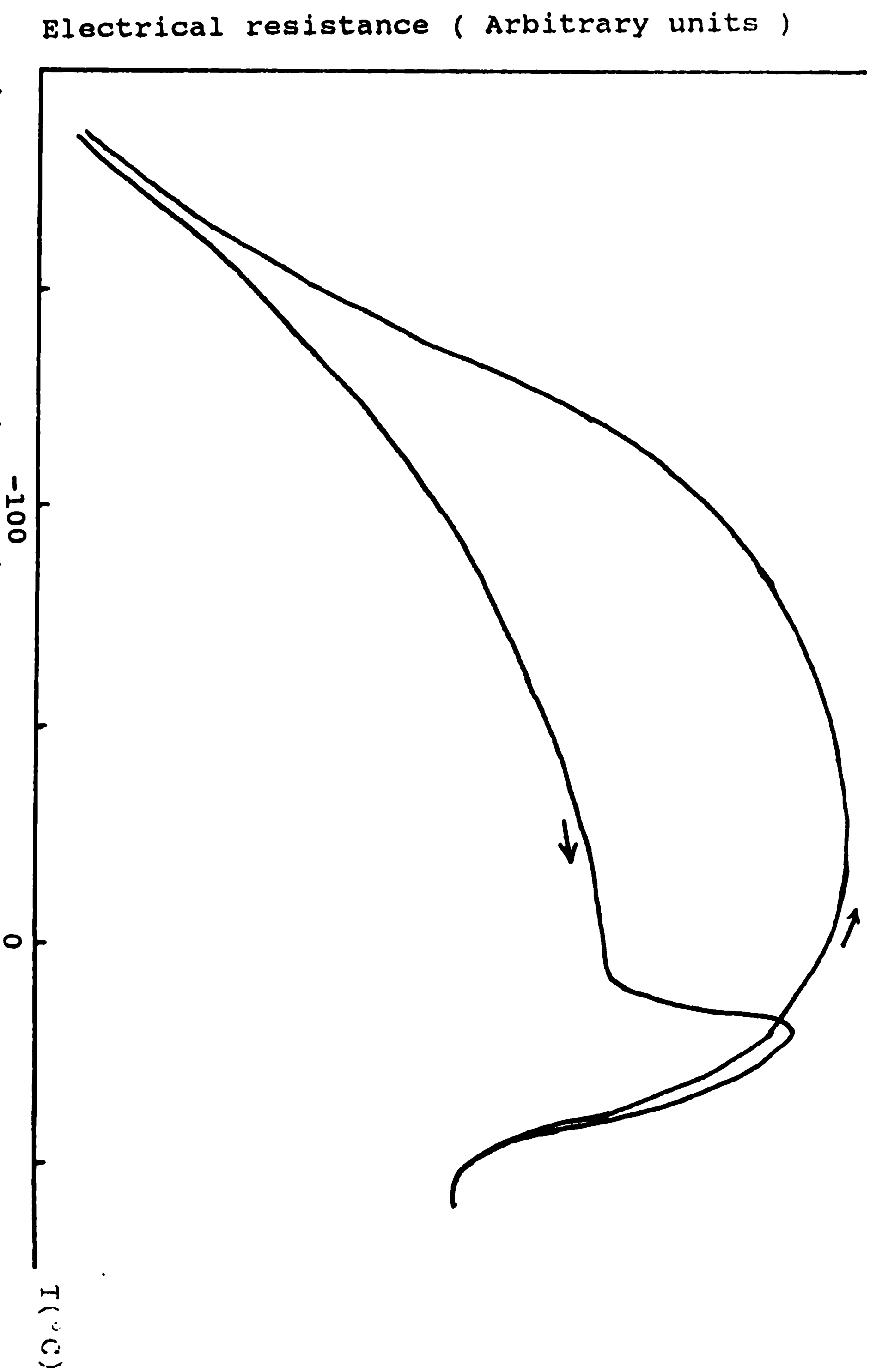

Fig. 14(b). Electrical resistance vs. temperature curve of thermal cycle 90 between +60°C and -196°C, specimen 400°C-10hrs-water.

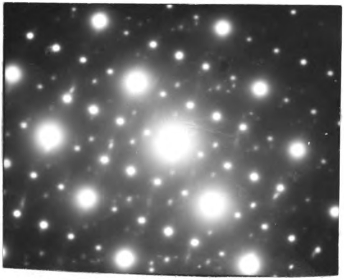

14(c)

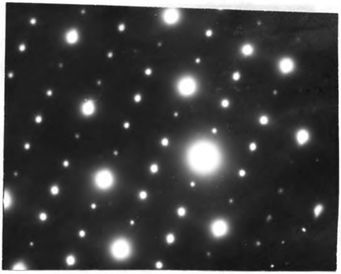

14(d)

Figs. 14(c) to 14(h). Transmission eletron micrograph and diffraction of specimen 400° C-10hrs-water
14(c) [110] B2 zone diffraction pattern with 1/3(101) extra spots
14(d) [110] B2 zone diffraction pattern with 1/3(111) extra spots

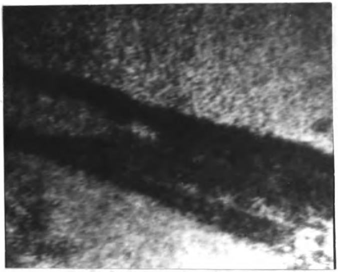

14(e)

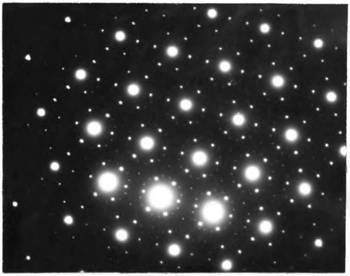

14(f)

14(e) Bright field micrograph corresponding to 14(d), mag. 50,000x
14(f) [111] B2 micrograph with 1/3(011) extra spots and small spots from precipitates

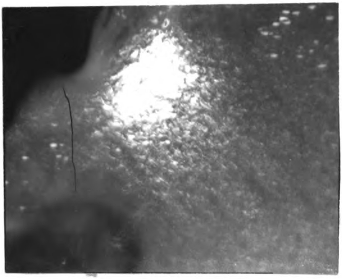

14(g)

14(h)

14(g) Dark field micrograph precipitates, mag. 100,000x
14(h) Bright field micrograph corresponding to 14(g), mag. 100,000x

period, e.g. 4hrs, its effect will become very weak probably because Ni and Ti achieve the equilibuium concentration in matrix. Since the precipitates are not too small, the back stress created by them are not large enough to obstruct the martensite formation.

D) Effect of cooling rate

Water quenching and air cooling were used after aging treatments in this study in order to measure the cooling rate effect on TiNi alloys. The aging temperatures used were 900° C and 400° C, while aging time was 1 hour. Electrical resistance vs. temperature curves of 900° C-1hr-air and 400° C-1hr-air are plotted in Fig. 15(a) and Fig. 16(a) respectively, and the corresponding transition temperatures are summarized in Table 1.

1) 900° C-1hr-air

The resistance curve of 900° C-1hr-air is totally different from that of As-quenched specimen. Upon cooling, there is a broad peak around -134° C followed by further increase in resistance. The structure of this specimen in the temperature region from room temperature to liquid nitrogen temperature is thought to be in the premartensitic transformation zone and the hysteresis shown may correspond to the first hysteresis before Ms in specimen 400° C-1hr-water. Since the Td is about -70° C, much lower than room temperature, the 1/3 position extra diffraction spots in reciprocal lattice are very weak and diffuse (See Fig. 15(b)).

The relatively slow cooling from 900°C can supply another opportunity for low temperature aging. The formation of precipitates is the result of this low temperature aging effect (See Fig 15(c)). The Ms and other transition temperatures are depressed by air cooling, probably due to the precipitates growing along the grain boundaries. The low temperature aging effect affects the specimen only during a very short time period, a few seconds roughly. The nucleation of precipitates favorably appears at areas of structural defect in order to lower the nucleation energy. Therefore, short-time low-temperature aging encourages the precipitates to aggregate along grain boundaries. The longitudinal dimension of the precipitates is up to 300 nm. The precipitate density is relatively low in the matrix and the extent of decrease in Ni concentration is somewhat limited. Though the decrease in Ni concentration could raise the Ms temperature, the influence of the grain boundary precipitate aggregation could be even larger and consequently dominant. Therefore, the Ms temperature is depressed.

2) 400°C-1hr-air

Comparing specimens 400°C-1hr-air and 400° C-1hr-water the shape of the resistance curves as well as Ms, Tp and Td, are very similar to each other. Furthermore, The

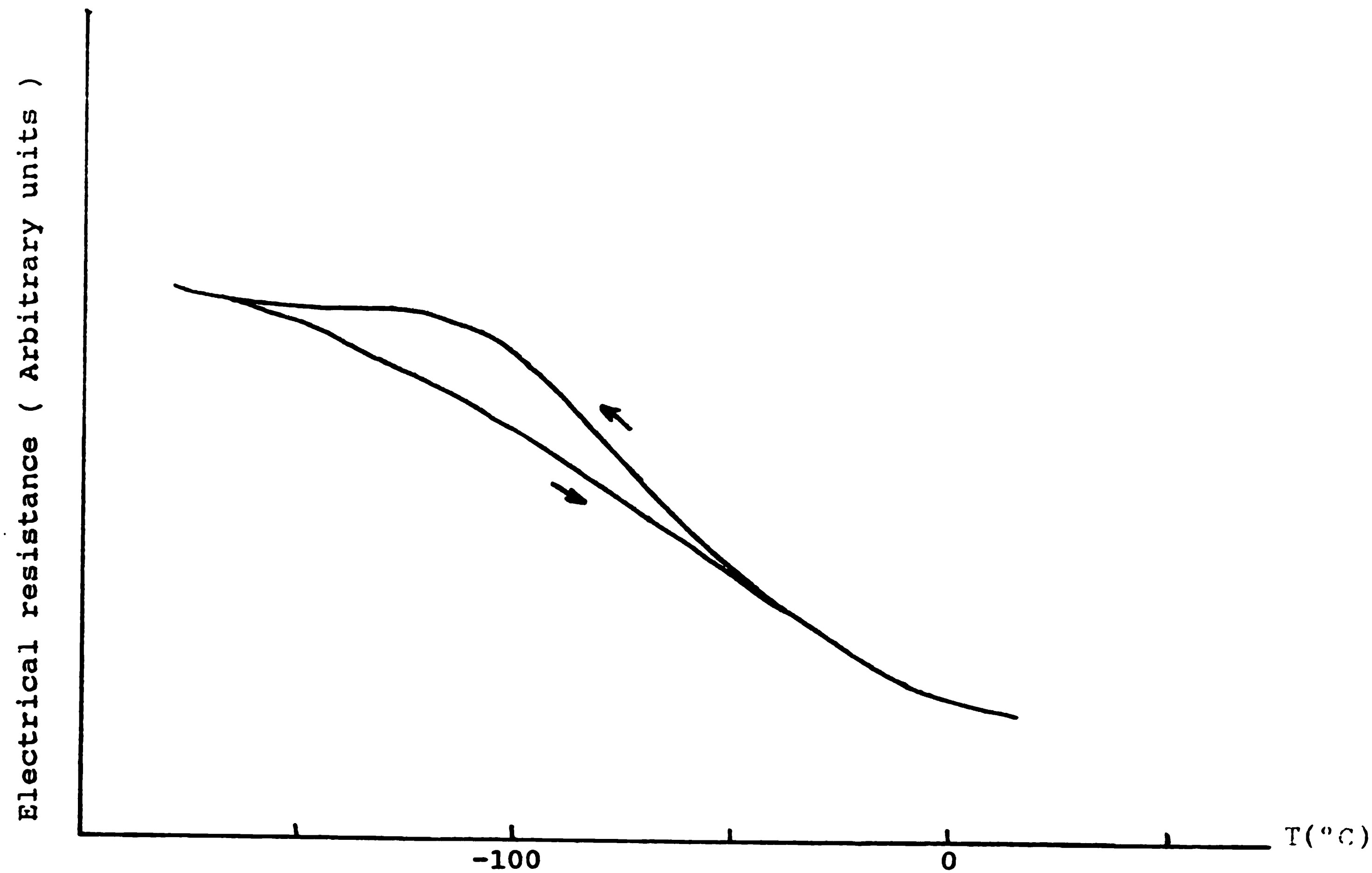

Fig. 15(a). Electrical resistance vs. temperature curve of thermal cycle 1 between +60° C and -196° C, specimen 900° C-1hr-air.

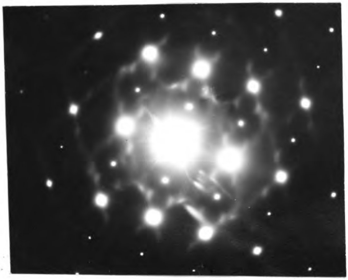

15(b)

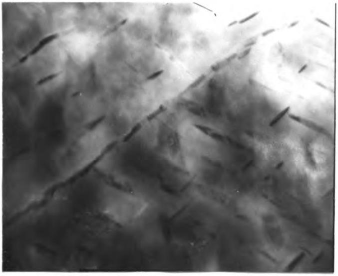

15(c)

Figs. 15(b) to 15(c). Transmission eletron micrograph and diffraction pattern of specimen 900° C-1hr-air
15(b) [210] B2 zone diffraction patterns with diffuse streaks
15(c) Bright field micrograph showing precipitates aggregating along grain boundary, mag. 60,000x

premartensitic transformation is enhanced in specimen 400° C-1hr-air, verifible by the clear 1/3 position extra diffraction spots (See Fig. 16(b)), while large quantity but small size (20nm x 2nm) precipitates are formed (See Fig. 16(c)). As mentioned before, the formation of precipitates will decrease the Ni concentration in the matrix and consequently raise the Ms temperature.

Since Td temperature (+25°C) is higher than room temperature, the specimen will be in the commensurate phase. The needle-like domains observed are shown in Fig. 16(d) and their corresponding selected area diffraction pattern is shown in Fig. 16(e). Unfortunately, the restriction of objective lens aperture size makes the dark field observation unfeasible. According to the studies of resistance curve and TEM observation, it can be concluded that the cooling rate has no significant effect on speciens aged at 400° C. This conclusion is totally different from that reached by observations of specimens aged at 900° C, probably due to the absence of lower temperature (< 400° C) aging effect.

E) Effect of thermal cycling

Three specimens, including As-quenched, 400° C-1hr-water and 400° C-10hrs-water, were chosen to undergo thermal cycling from +60° C to -196° C (liquid nitrogen temperature) and their transition temperatures for cycle 1, 30 and 90

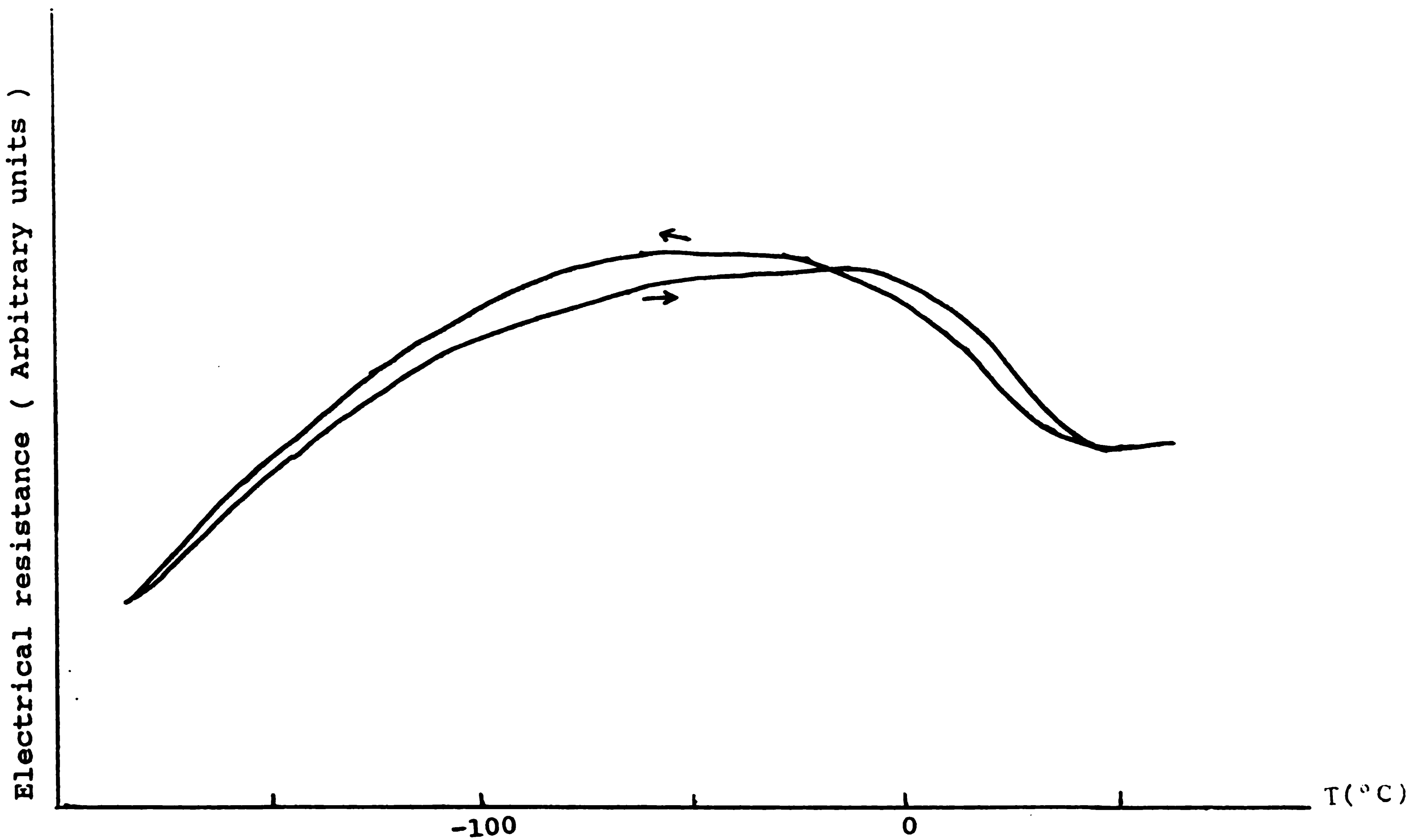

Fig. 16(a). Electrical resistance vs. temperature curve of thermal cycle 1 between +60°C and -196°C, specimen 400°C-1hr-air.

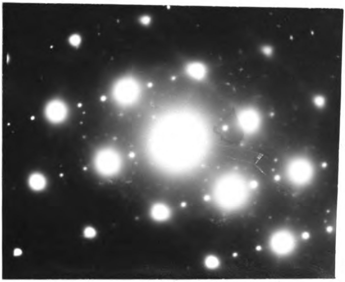

16(b)

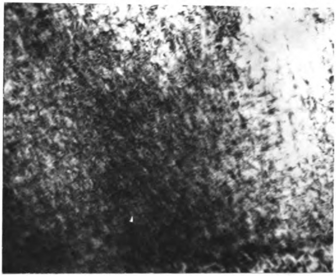

16(c)

16(b) [111] B2 zone diffraction pattern with 1/3(011) extra spots and small spots from precipitates.
16(c) Bright field micrograph showing small precipitates,mag. 150,000x

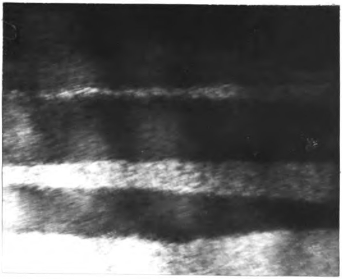

16(d)

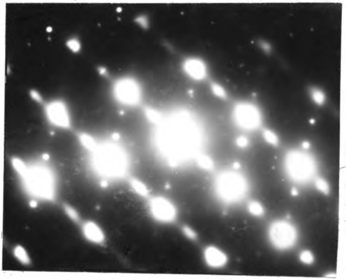

16(e)

16(d) Bright field micrograph showing suspected needle-like domains, mag. 50,000x
16(e) Selected area diffraction pattern corresponding to 16(d)

are summarized in Table 3.

1) As-Quenched

The increase of thermal cycles can depresses Ms temperature from -94° C to -104° C in 90 cycles while Mf, As and Af temperatures do not exhibit such an evident difference. The electrical resistance vs. temperature curve of the first cycle is plotted in Fig. 1 (a). With the increase of thermal cycles, the resistance hysteresis moves towards lower temperatures and the resistance peak at Ms temperature becomes higher. Similarly, upon heating, the resistance peak at Af temperature of cycle 90 is higher than that of cycle 1. The change of Ms temperature arises from the dislocations introduced during thermal cycling. Dislocations impede the martensite formation, consequently depressing the Ms temperature.

2) 400 C-1hr-water

The depression of Ms temperature in this specimen due to thermal cycling is much less than that of the As-quenched specimen. The similarity of resistance curves of cycle 1 and cycle 90 indicates that the effect of thermal cycling on 400° C-1hr-water is very little. The resistance curve of thermal 90 is plotted in Fig. 1(b).

The precipitates formed during aging may obstruct the mobility of dislocation. Therefore, the effect arising from dislocations on the martensite formation could be partially or almost totally eliminated.

Table 3. Thermal cycling effect on transition temperatures

Specimen	Cycle	Ms	Mf	As	Af	Tp	Td(°C)
As-quenched	1	-94	<-196	-82	-52	+30	-70
	30	-99	<-196	-82	-54	+28	-72
	90	-104	<-196	-84	-56	+28	-72
400°C-1hr-water	1	-38	<-196	<-196	-27	+49	+28
	30	-42	<-196	<-196	-30	+49	+28
	90	-40	<-196	<-196	-23	+49	+28
400°C-10hrs-water	1	-20	<-196	+8	+21	+54	+36
	30	-22	<-196	+8	+21	+54	+35
	90	-22	<-196	+10	+20	+53	+37

3) 400 C-10hrs-water

For specimen 900 C-10hrs-water, the Ms temperature is depressed with increasing thermal cycles though the difference is very little, from -20° C to -22° C. Cycle 90 is plotted in Fig. 11(b). The resistance hysteresis is depressed with the increasing of thermal cycles. This phenomenon is inconsistent with the result obtained from As-quenched specimen. It can be interpreted by proposing that the rearrangement of dislocations during martensitic transformation is obstructed by the coarse precipitates in this specimen.

F) Effect of cold rolling

The effect of cold work was studied by cold rolling the As-quenched specimens to 10%, 20% and 40% reduction in thickness, (original thickness 0.5mm). The corresponding electrical resistance vs. temperature curves are plotted in Figs. 17, Fig. 18(a) and Fig. 19. The As-quenched specimen is a very ductile alloy and no cracks can be seen when cold rolled up to 40 % reduction in thickness.

The resistance curves of C-R-10% and C-R-20% are very similar to each other, having very flat resistance hysteresis and no abrupt decreases at Ms temperatures. The flatness of the curve makes it difficult to measure the exact transition temperatures. The Ms temperature is depressed by introducing a large quantity of dislocations which partially or completely prevent the stable reorientation or growth of the martensite plates. These dislocations also affect the mobility of other dislocations which are responsible of the plastic flow.

The resistance curve of C-R-40% is nearly a straight line between +60° C and -196° C and the martensitic transformation was totally depressed in this seriously deformed specimen.

In Fig. 18(b), the bright field micrograph taken from C-R-20% shows some fine lamellar strain-induced martensite plates whose structure is monoclinic and a = 28.89nm, b = 41.20nm ,c = 46.22nm and β = 96.80° .

The boundaries of these strain-induced martensite lamellae are not expected to be mobile, because of dense dislocations along them. The dark field and bright micrographs of strain-induced martensite plates and their corresponding selected area diffraction pattern are shown in Figs. 18(c), 18(d) and 18(e). The morphology of martensite plates and their corresponding diffraction spots can be used to determine the twin plane(s).

In some other portions of the same specimen described above, the 1/3 extra diffraction is very clear and strong in some orientations (See Fig. 19(f)). Still, some B2 diffractions with diffuse streaks are observed (See Fig. 18(g)). Since Tp is about +20° C and Td is -46° C, the presence of commensurate phase could probably be due to the

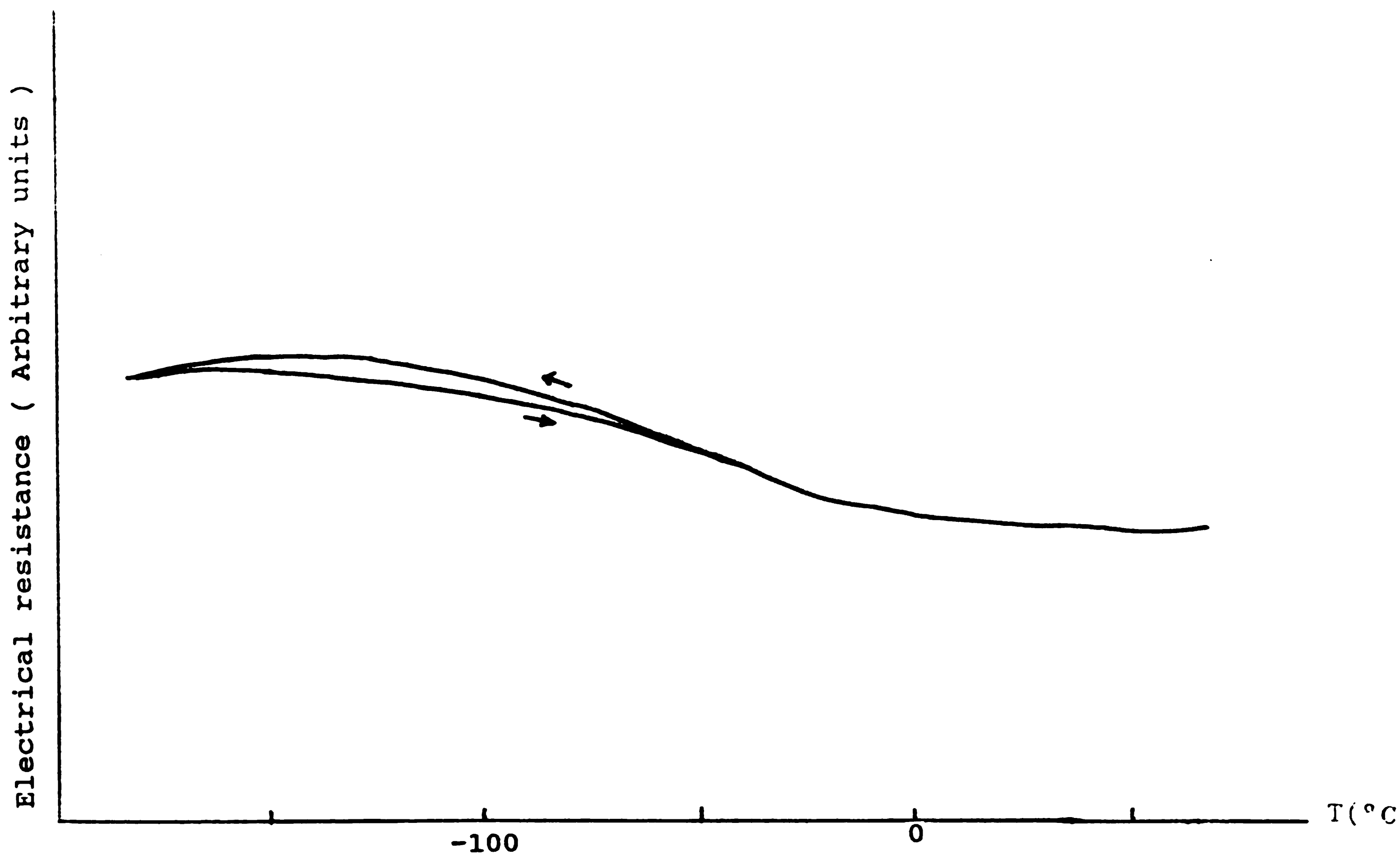

Fig. 17. Electrical resistance vs. temperature curve of thermal cycle 1 between +60° C and -196° C, specimen C-R-10%.

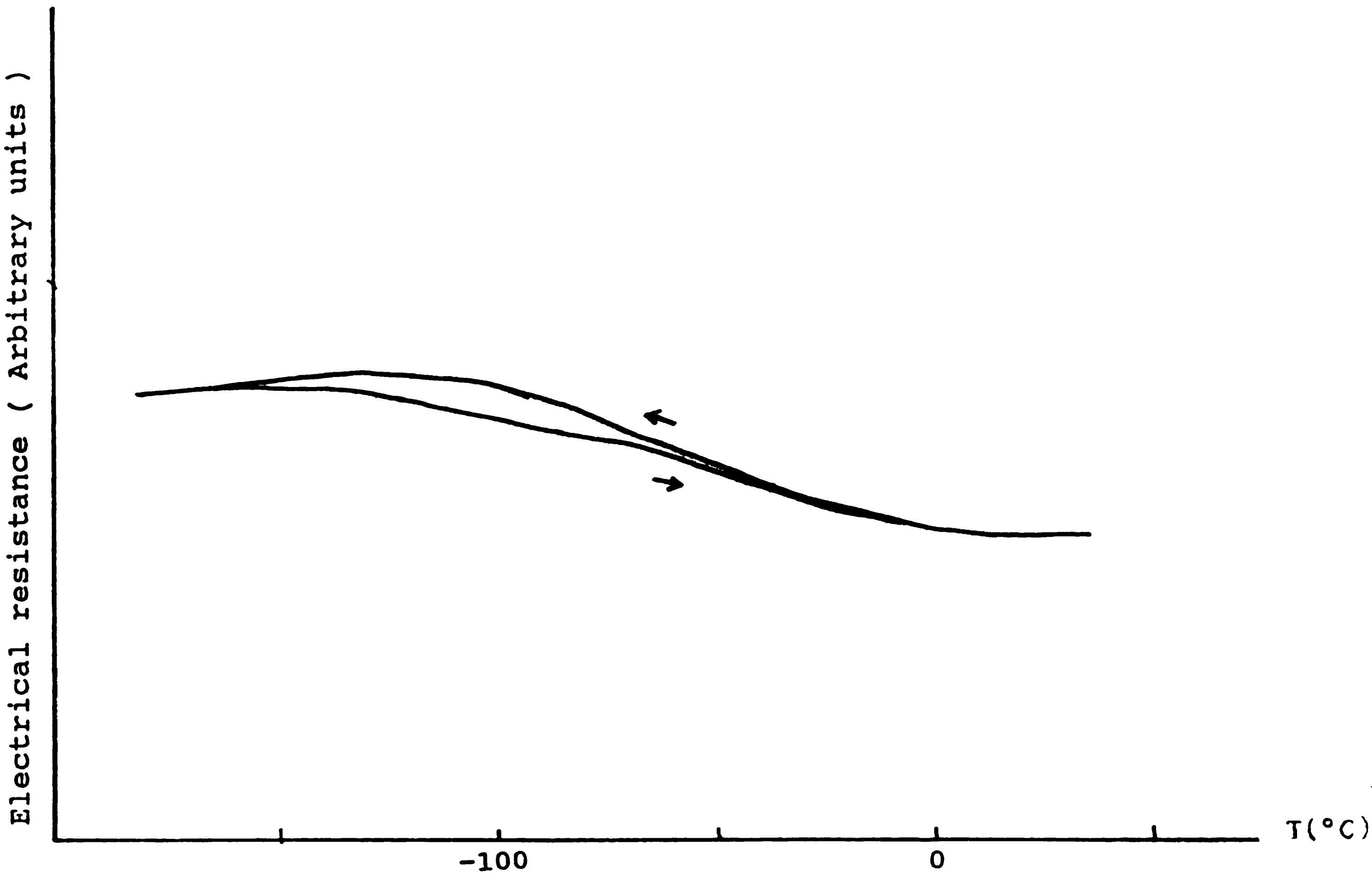

Fig. 18(a). Electrical resistance vs. temperature curve of thermal cycle 1 between +60° C and -196°C, specimen C-R-20%.

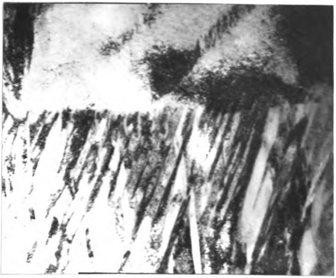

18(b)

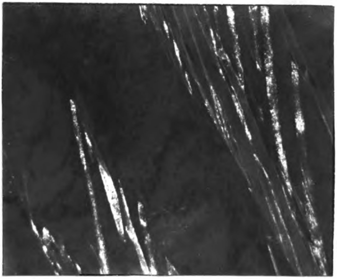

18(c)

Figs. 18(b) to 18(g). Transmission eletron micrographs and diffraction patterns of specimen C-R-20%
18(b) Bright field micrograph showing martensite plates, mag. 30,000x
18(c) Dark field micrograph showing martensite plates, mag. 50,000x

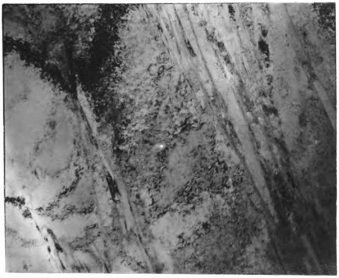

18(d)

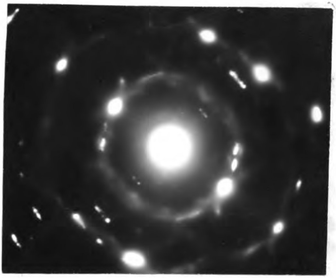

18(e)

18(d) Bright field ,icrograph corresponding to 18(c), mag. 50,000x
18(e) Selected area soffractgion corresponding to 18(c) and 18(d)

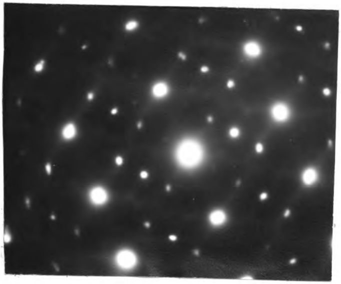

18(f)

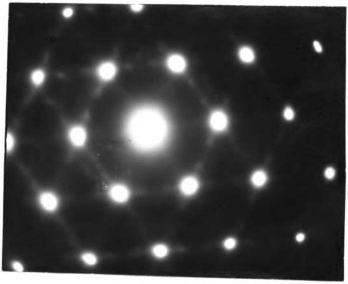

18(g)

18(f) [110] B2 zone diffraction with 1/3(112) extra spots
18(g) B2 zone diffraction with diffuse streaks

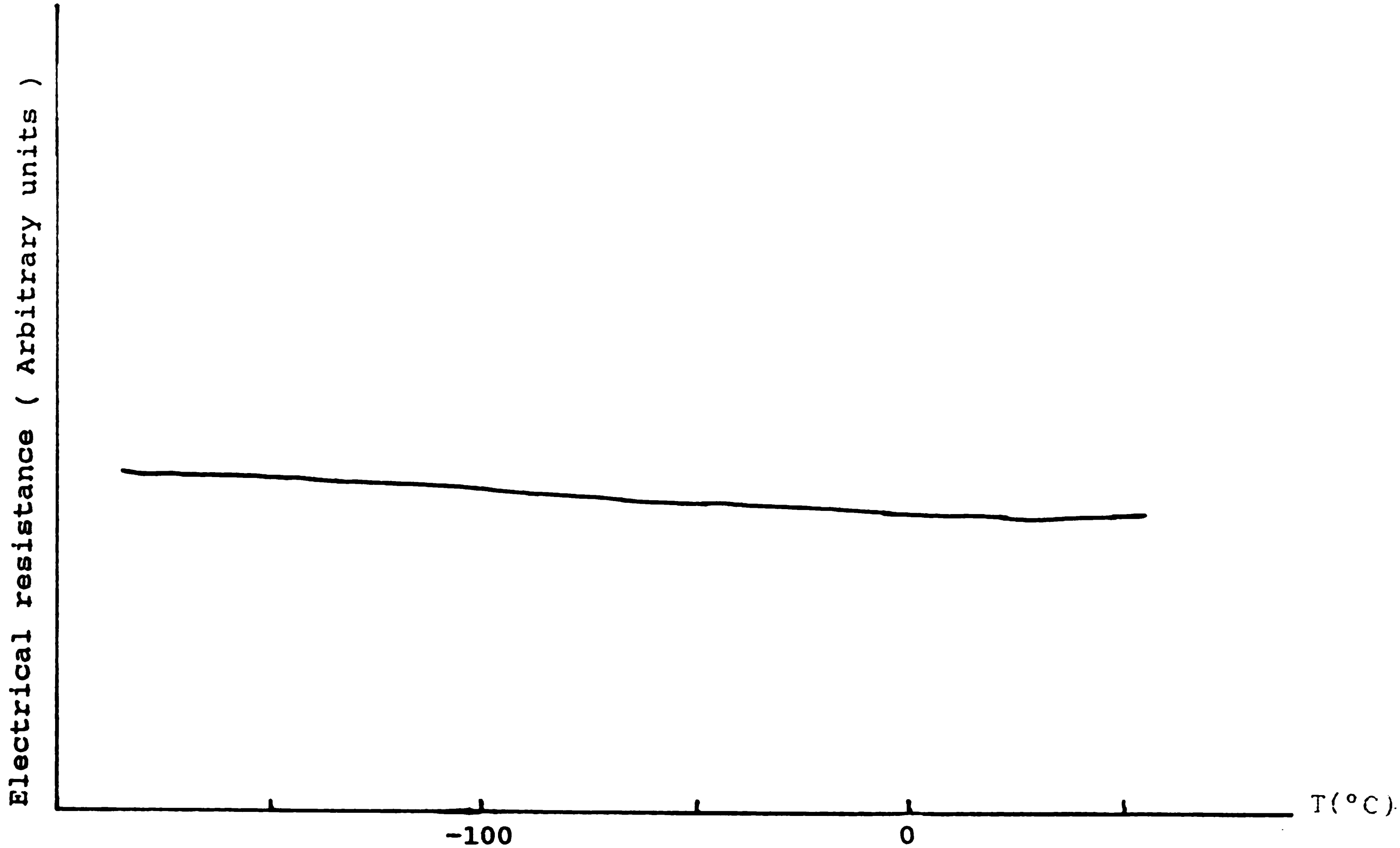

Fig. 19. Electrical resistance vs. temperature curve of thermal cycle 1 between +60° C and -196° C, specimen C-R-40%.

dislocations introduced by cold rolling. These dislocations can not only supply the nucleation cites for martensites but also for R phases (Suggested by Mercier et. al.). The R phases could probably nucleate preferentially on dislocations to lower the nucleation energy. It is suspected that some stress-induced R phases coexist with incommensurate parent phase and martensite plates. It is unfortunate that the dark field microscopy was restricted due to the size of second condenser lens aperture in the electron microscope.

G) Effect of annealing after cold rolling

The specimens used to study this effect were made using the same procedures as those for cold rolled specimens. These three cold rolled specimens were annealed at 500 C for 1 hour followed by water quenching. The specimens were denoted as C-R-10%--500° C-1hr-water, C-R-20%--500° C-1hr-water and C-R-40%--500° C-1hr-water, and their resistance curves were plotted in Fig. 20, Fig. 21(a) and Fig. 22. The transition temperatures obtained from these specimens are summarized in Table 2. For comparison, the transition temperatures of 500 C-1hr-water was also included in Table 2.

Annealing after cold rolling dramatically changes the resistance curves of these three cold rolled specimens make them very similar to one another. The effect on degree of deformation was almost removed by later annealing. Furthermore, the similarity of resistance curves and transition temperatures between 500°C-1hr-water and the "cold-rolled and annealed" specimens was very pronounced. A large number of dislocations were introduced by cold rolling, and these might act as barriers to the reorientation or growth of the martensite plates and also pin the other dislocations which are responsible for plastic flow. The effect of annealing after cold rolling is to create a dislocation substructure which could bar the growth of martensite plates, but allow easier reorientation of these plates.

Figs. 21(b) and 21(c) show some martensite plates in low magnification of specimen C-R-20%--500°--C-1hr-water. Dark field and bright field micrographs and their corresponding selected area diffraction pattern are shown in Figs. 21(d), 21(e) and 21(f) respectively. The precipitates observed in Fig. 21(e) also helped to raise the Ms temperature. An enlarged portion of a martensite plate shows some microtwins with different orientations (See Figs. 21(g) and 21(h)).

These microtwins are suspected of being responsible for the pseudoelasticity below Ms temperature. They cannot grow much on loading because of the existence of the dislocation substructure around them. Therefore, the microtwin could contract on releasing the stress in a

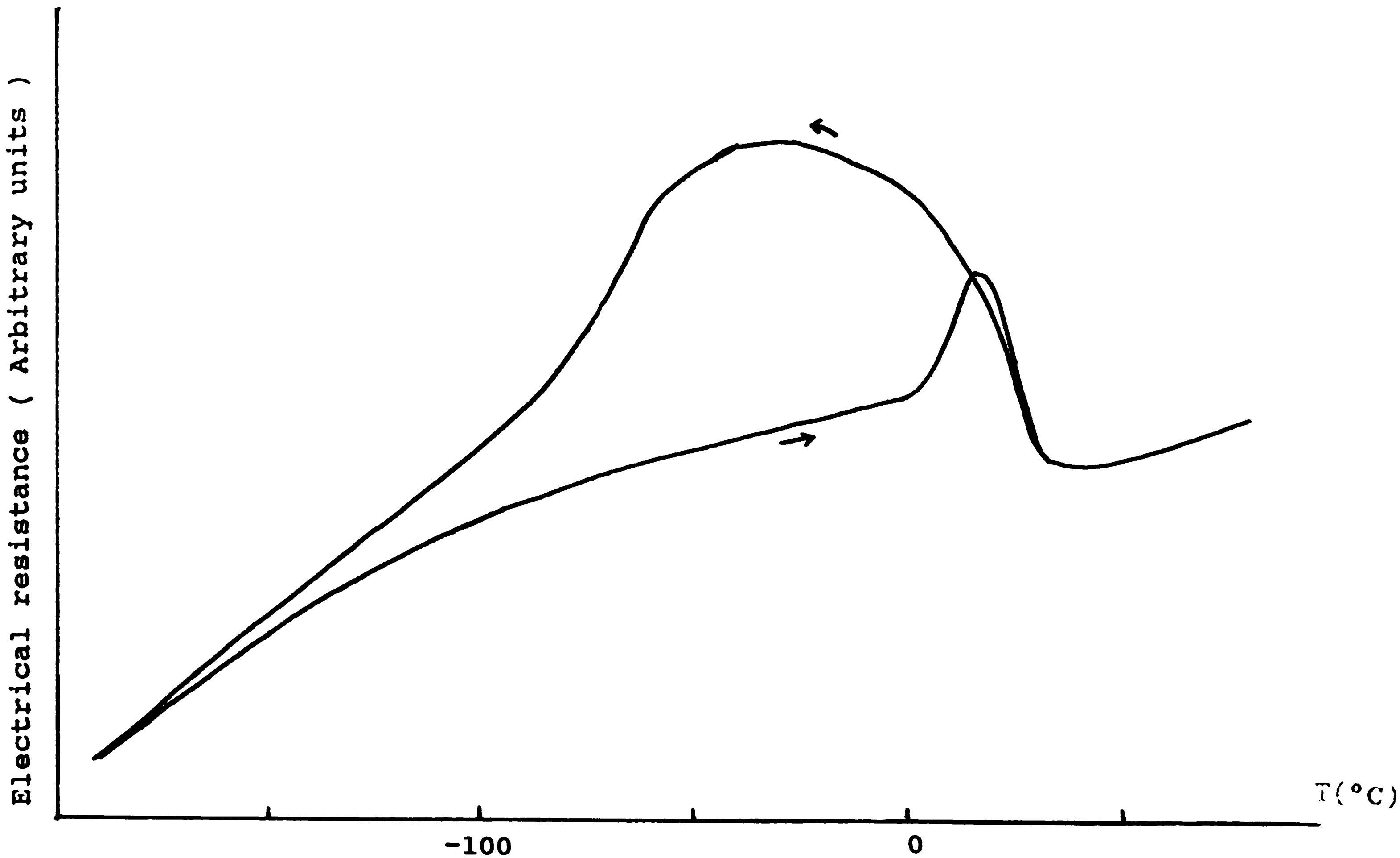

Fig. 20. Electrical resistance vs. temperature curve of thermal cycle 1 between +60°C and -196°C, specimen C-R-10%--500°C-1hr-water.

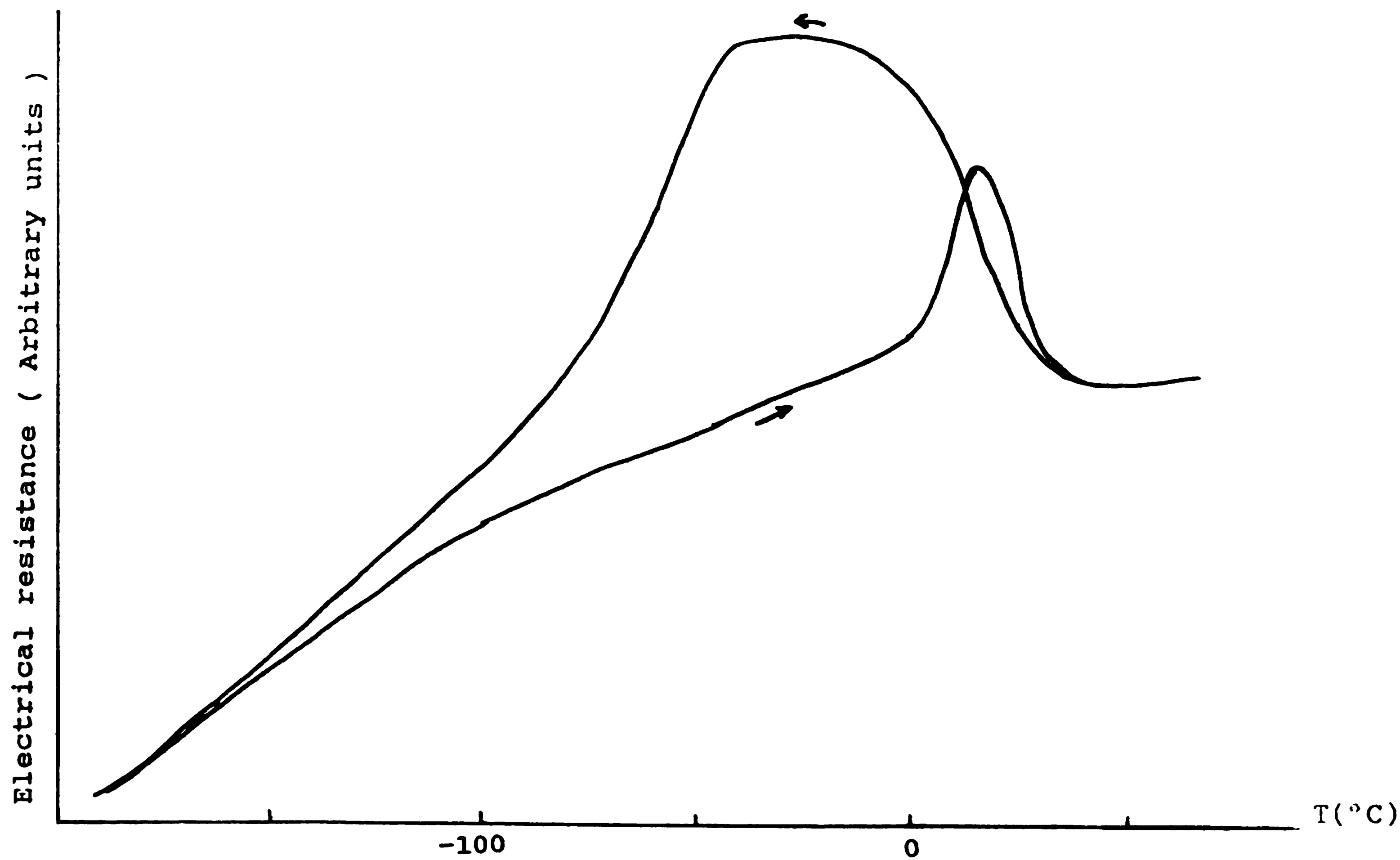

Fig. 21(a) Electrical resistance vs. temperature curve of thermal cycle 1 between +60°C and -196°C, specimen C-R-20%--500°C-1hr-water.

21(b)

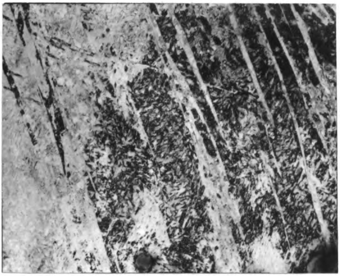

21(c)

Figs. 21(b) to 21(h). Transmission eletron micrographs and diffraction patterns of specimen C-R-20%--500° C-1hr-water 21(b) and 21(c). Bright field micrographs showing martensite plates, mag. 12,000x

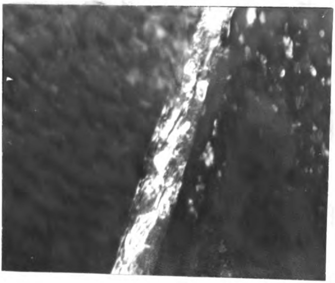

21(d)

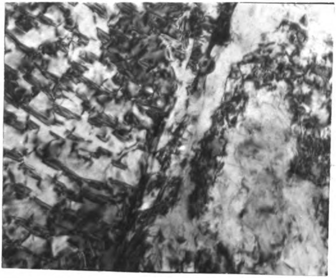

21(e)

21(d) Dark field micrograph showing a martensite plate, mag. 100,000x
21(e) Bright field micrograph corresponding to 21(d). Some precipitates are also shown.

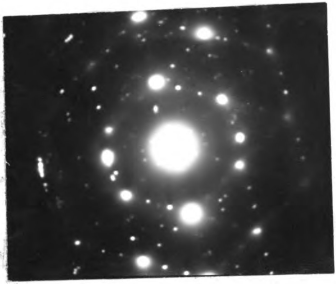

21(f)

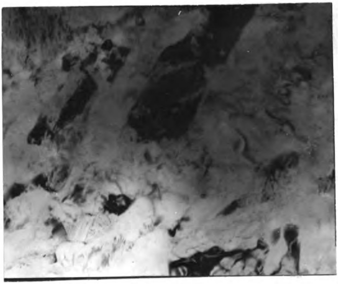

21(g)

21(f) Selected area diffraction corresponding to 21(d) and 21(e)
21(g) Bright field micrograph showing martensite plate, mag. 80,000x

21(h)

21(h) Enlarged bright micrograph from 21(g) showing some microtwins with different orientations

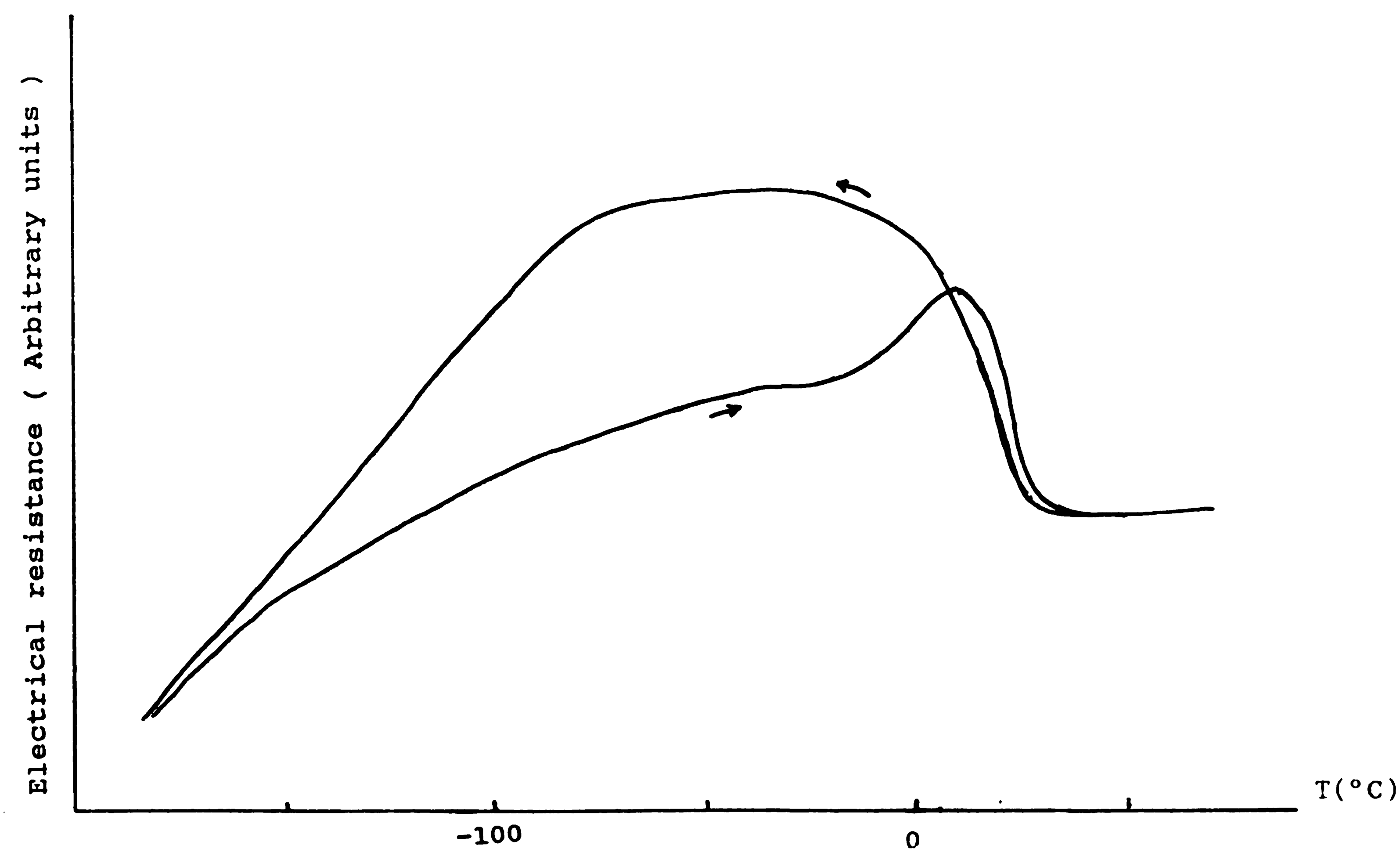

Fig. 22. Electrical resistance vs. temperature curve thermal cycle 1 between +60°C and -196°C, specimen C-R-40%--500°C-1hr-water.

reversible, way with driving force arising from the repulsive force between twinning dislocations themselves or twinning dislocations and barrier-forming dislocations.

IV. SUMMARY

The martensitic as well as premartensitic transformation of Ni rich TiNi alloys could be affected by several variables, such as aging time, aging temperature, cooling rate, cold work and thermal cycling, etc. The effect of different variables has been evaluated in this study. The controlling factors of martensitic and premartensitic transformations are the formation of precipitates and the introduction of dislocations due to the change of the variables described above.

Regarding aging temperature effect, the electrical resistance vs. temperature curves of 500°C-1hr-water and 400° C-1hr-water changed greatly due to the nucleation and growth of precipitates, and consequently caused changes in the matrix composition. This effect raised the Ms temperature. From 800° C to 600° C, the lower the aging temperatures, the higher the Ms temperatures were.

As concerns aging time effect, premartensitic effect was enhanced by longer aging treatments. The formation of precipitates and their subsequent growth probably attained equilibrium with the matrix when aged for more than 4 hours. Specimen 500° C-10 hrs-water had the largest precipitates among all specimens observed under TEM.

For cooling rate effect, different results were obtained from specimens 900° C-1hr-air and 400° C-1hr-air. Air-cooled specimen 900° C-1hr-air had a different resistance curve when compared to the As-quenched specimen, probably due to precipitates aggregation along the grain boundaries. Cooled from 400°C, specimen 400°C-1hr-air did not undergo lower temperature aging, and its resistance curve was very similar to that of specimen 400°C-1hr-water.

Different results were observed for the thermal cycling effect. The As-quenched specimen, after 90 thermal cycles, had lower Ms temperature because of the formation of dislocations. Specimens 400°C-1hr-water and 400° C-10hrs-water did not manifest obvious changes in their transition temperatures. This phenomenon could due to precipitates obstructing the mobility of dislocations.

As for cold rolling effect, all the tested specimens were deformed so seriously that their resistance hystereses were depressed to temperatures close to or lower than liquid nitrogen temperature. The high density of dislocation obstructed the reorientation and the formation of martensites. Strain-induced martensites were also observed.

As concerns the "cold rolling and annealing" effect, cold-rolled specimens had their resistance curves affected by annealing treatments. The formation of precipitates and dislocation substructures were suspected to be the controlling factors. All of the resistance curves of tested specimens were similar to one another and close to that of specimen 500°C-1 hr-water. The cold rolling effect was partially or almost eliminated by the annealing.

The effect of thermomechnical treatments on transformation behavior of a TiNi alloy was studied in this research. The martensitic and premartensitic transformation behaviors of the TiNi alloy are very sensitive to the thermomechanical treatments performed to the specimens. Dramatic changes in resistance curves of cold-rolled specimens after subsequent annealing treatments were observed. It was concluded that the premartensitic transformation was enhanced by the aging treatments.

LIST OF REFERENCES

1. C. M. Wayman, J. Metals, 32, 129 (1980).
2. M. Nishida and T. Honma, Scripta Met., 18, 1293 (1984).
3. M. Nishida and T. Honma, Scripta Met., 18, 1299 (1984).
4. M. Nishida and C.M. Waymen, Scripta Met., 18, 1299 (1984).
5. S. Miyazaki, T. Tatsumi and S. Nenno, Supplement to Journal de physique, 43, C4-261 (1982).
6. C. M. Hwang, M. Meichle, B. Salamon and C. M. Waymen, Phil Mag. A, 47, No.1, 9 (1983).
7. C. M. Hwang, M. Meichle, B. Salamon and C. M. Waymen, Phil Mag. A, 47, No. 1, 31 (1983).
8. C. M. Hwang, M. B. Salamon and C. M. Waymen, Phil Mag. A, 47, No. 2, 177 (1983).
9. C. M. Hwang and C. M. Waymen, Scripta Met., 17, 385 (1983).
10. C. M. Hwang and C. M. Waymen, Scripta Met., 17, 381 (1983).
11. C. M. Hwang and C. M. Waymen, Scripta Met., 17, 1449 (1983).
12. C. M. Hwang and C. M. Waymen, Acta Met., 32, No.1, 183 (1984).
13. P. Moine, G. M. Michal and R. Sinclair, Acta Met., 30, 109 (1982).
14. P. Moine, G. M. Michal and R. Sinclair, Acta Met., 30, 125 (1982).
15. P. Moine, E. Goo and R. Sinclair, Supplement to Journal de Physique, 43, C4-273 (1982).

16. K. M. Knowles and D. A. Smith, Acta Met., 29, 101 (1981).

17. S. R. Zijlstra, J. Beijer and J. A. Klostermann, J. Mater. Sci. 9, 145 (1974).

18. M. Nishida and C. M. Waymen, Scripta Met., 19, 983 (1985).

19. P. Moine, E. Goo and R. Sinclair, Supplement to Journal de Physique, 43, C4-273 (1982).

20. T. Honma, M. Matsumoto, Y. Shugo, M. Nishida and I. Yamazaki, Titanium Science and Technology, R. Jaffe ed., 3, 1433 (1980).

21. T. Tadaki and C. M. Waymen, Scripta Met., 17, 1449 (1983).

22. K. N. Melton and O. Mercier, Acta Met., 29, 393 (1981).

23. S. Miyazaki, T. Imai, Y Igo and K. Otsuka, Met Trans., A, 17A,115 (1986).

24. T. Saburi, T. Tatsumi and S. Nenno, Supplement to Journal de Physique, 43, C4-261 (1982).

25. P. Moine, E. Goo and R. Sinclair, Scripta Met., 18, 1143 (1984).

26. S. Miyazaki and K. Otsuka, Met Trans., A. 17A, 53 (1986).